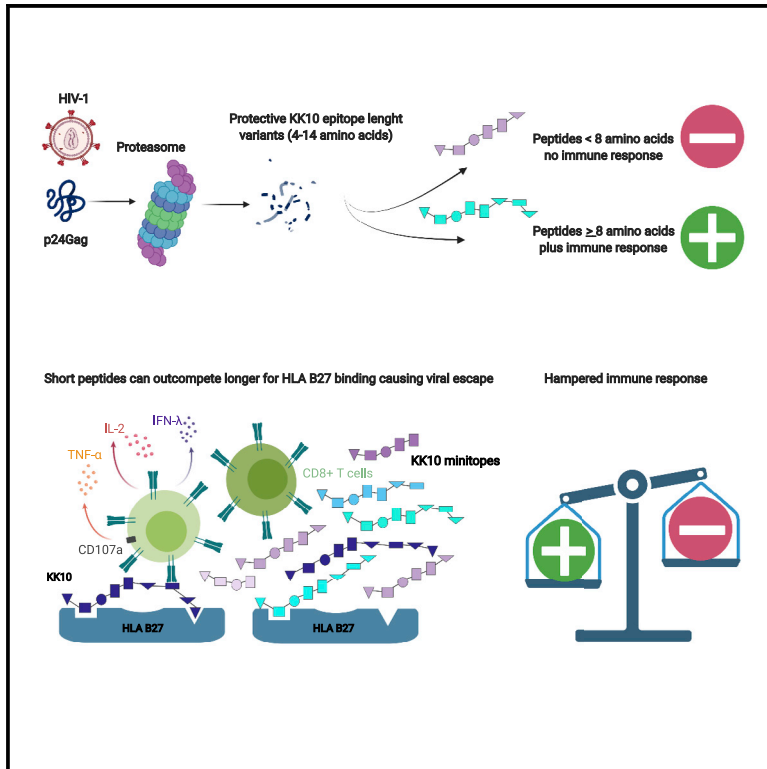


Epitope length variants balance protective immune responses and viral escape in HIV-1 infection

Graphical abstract



Authors

Phillip Pymm, Stefan Tenzer, Edmund Wee, ..., Peter van Endert, Maria Harkiolaki, Astrid K.N. Iversen

Correspondence

astrid.iversen@ndcn.ox.ac.uk

In brief

Pymm et al. investigate how HIV-1 adapts to intracellular epitope processing preferences to escape cellular immune responses. Using the processing of the HLA-B*27:05-restricted epitope KK10 as a model, they find that processing generates several epitope length variants and demonstrate that peptide competition can dampen cellular immune responses in the context of HLA-B*27:05.

Highlights

- Proteasomal activity creates many length variants of the protective KK10 HIV-epitope
- All KK10 length variants bind HLA-B*27:05 through a conserved N-terminal motif
- Short KK10 length variants outcompete immunogenic, longer variants for HLA binding
- Epitope variant competition balances protective immune responses and viral escape



Article

Epitope length variants balance protective immune responses and viral escape in HIV-1 infection

Phillip Pymm,^{1,2} Stefan Tenzer,³ Edmund Wee,¹ Mirjana Weimershaus,^{4,5} Anne Burgevin,^{4,5} Simon Kollnberger,⁶ Jan Gerstoft,⁷ Tracy M. Josephs,⁸ Kristin Ladell,⁶ James E. McLaren,⁶ Victor Appay,^{9,10} David A. Price,^{6,11} Lars Fugger,^{1,12} John I. Bell,¹³ Hansjörg Schild,³ Peter van Endert,^{4,5} Maria Harkiolaki,^{14,15} and Astrid K.N. Iversen^{1,16,*}

¹Nuffield Department of Clinical Neurosciences, Division of Clinical Neurology, Weatherall Institute of Molecular Medicine, John Radcliffe Hospital, University of Oxford, Headley Way, Oxford OX3 9DS, UK

²Walter and Eliza Hall Institute of Medical Research, University of Melbourne, 1G Royal Parade, Parkville, VIC 3052, Australia

³Institute of Immunology, University Medical Center of the Johannes-Gutenberg University of Mainz, Langenbeckstrasse 1, 55131 Mainz, Germany

⁴Institut National de la Santé et de la Recherche Médicale, Unité 1151, Université Paris Descartes, Sorbonne Paris Cité, Hôpital Necker, 149 Rue de Sévers, 75015 Paris, France

⁵Centre National de la Recherche Scientifique, UMR8253, Université Paris Descartes, Sorbonne Paris Cité, Hôpital Necker, 149 Rue de Sévers, 75015 Paris, France

⁶Division of Infection and Immunity, Cardiff University School of Medicine, University Hospital of Wales, Heath Park, CF14 4XN Cardiff, UK

⁷Department of Infectious Diseases, Rigshospitalet, The National University Hospital, Blegdamsvej 9, 2100 Copenhagen, Denmark

⁸Drug Discovery Biology, Monash Institute of Pharmaceutical Sciences, 381 Royal Parade, Parkville, VIC 3052, Australia

⁹Institut National de la Santé et de la Recherche Médicale, Unité 1135, Centre d'Immunologie et des Maladies Infectieuses, Sorbonne Université, Boulevard de l'Hôpital, 75013 Paris, France

¹⁰International Research Center of Medical Sciences, Kumamoto University, 2-2-1 Honjo, Chuo-ku, Kumamoto City 860-0811, Japan

¹¹Systems Immunity Research Institute, Cardiff University School of Medicine, University Hospital of Wales, Tenovus Building, CF14 4XN Cardiff, UK

¹²Medical Research Council Human Immunology Unit, Weatherall Institute of Molecular Medicine, University of Oxford, John Radcliffe Hospital, OX3 9DS Oxford, UK

¹³Office of the Regius Professor of Medicine, The Richard Doll Building, University of Oxford, Old Road Campus, OX3 7LF Oxford, UK

¹⁴Structural Biology Group, Wellcome Trust Centre for Human Genetics, University of Oxford, Old Road Campus, OX3 7LF Oxford, UK

¹⁵Diamond Light Source, Harwell Science and Innovation Campus, Fermi Avenue, OX11 0DE Didcot, UK

¹⁶Lead contact

*Correspondence: astrid.iversen@ndcn.ox.ac.uk

<https://doi.org/10.1016/j.celrep.2022.110449>

SUMMARY

Cytotoxic T lymphocyte (CTL) and natural killer (NK) cell responses to a single optimal 10-mer epitope (KK10) in the human immunodeficiency virus type-1 (HIV-1) protein p24Gag are associated with enhanced immune control in patients expressing human leukocyte antigen (HLA)-B*27:05. We find that proteasomal activity generates multiple length variants of KK10 (4–14 amino acids), which bind TAP and HLA-B*27:05. However, only epitope forms ≥ 8 amino acids evoke peptide length-specific and cross-reactive CTL responses. Structural analyses reveal that all epitope forms bind HLA-B*27:05 via a conserved N-terminal motif, and competition experiments show that the truncated epitope forms outcompete immunogenic epitope forms for binding to HLA-B*27:05. Common viral escape mutations abolish (L136M) or impair (R132K) production of KK10 and longer epitope forms. Peptide length influences how well the inhibitory NK cell receptor KIR3DL1 binds HLA-B*27:05 peptide complexes and how intraepitope mutations affect this interaction. These results identify a viral escape mechanism from CTL and NK responses based on differential antigen processing and peptide competition.

INTRODUCTION

Human leukocyte antigen (HLA)-B*27:05 and HLA-B*57:01/03 show robust protective effects in human immunodeficiency virus type-1 (HIV-1) infection (Goulder and Walker, 2012). The positive clinical impact of HLA-B*27:05 is linked to CD8⁺ cytotoxic T

lymphocyte (CTL) responses directed against a single HIV-1 epitope in the viral capsid protein p24 Gag (¹³¹KRWIILGLNK¹⁴⁰) (Feeney et al., 2004; Goulder et al., 1997; Goulder and Watkins, 2008; Nixon et al., 1988). This optimal 10-mer epitope, termed KK10, was defined *in vitro* using progressively truncated peptides to elicit functional responses among peripheral blood



mononuclear cells (PBMCs) isolated from HLA-B*27:05⁺ patients (Brander and Walker, 1996; Gnann et al., 1987). Weaker clinical benefits have been associated with the activity of inhibitory natural killer (NK) cells in HLA-B*27:05⁺ patients (Martin and Carrington, 2013; Martin et al., 2007). However, it remains unclear precisely how cellular immune responses directed against a single HIV-1 epitope can delay the onset of acquired immune deficiency syndrome (AIDS) (Goulder and Walker, 2012; Goulder and Watkins, 2008).

Several attributes of KK10-specific CTL responses have been associated with effective immune control of viral replication and slow disease progression, including enhanced antigen sensitivity and polyfunctionality, which in turn have been linked to increased clonal turnover and the expression of particular T cell receptors (TCRs) (Almeida et al., 2007; Chen et al., 2012; Wilson et al., 1998). Other factors may also determine the functional properties of KK10-specific CTLs (Joglekar et al., 2018). However, these studies were focused on the recognition of the optimal KK10 epitope, which is produced in small amounts by human constitutive proteasomes or immunoproteasomes during *in vitro* digestion of longer peptides from p24 Gag (Steers et al., 2011; Tenzer et al., 2009, 2014). In contrast, a range of truncated peptides, known as KK10 minitopes (Tenzer et al., 2009), and C-terminally-extended KK10 epitope forms are produced in abundance (Steers et al., 2011; Tenzer et al., 2009, 2014). Some of these KK10 epitope forms were tested previously in functional assays and failed to elicit functionally superior CTL responses (Tenzer et al., 2009). A structure of the HLA-B*27:05-KK10 complex revealed N-terminal binding of the residue at P2 (R132, or R2_{peptide}) in the B pocket, hydrophobic interactions in the E pocket, and C-terminal binding of K10_{peptide} in the F pocket (Stewart-Jones et al., 2005a). However, it remains unclear whether and to what extent truncated and C-terminally-extended KK10 epitope forms can bind HLA-B*27:05.

CTL-induced viral escape mutations can impose fitness costs that suppress HIV-1 replication (Gao et al., 2005; Kiepiela et al., 2007; Migueles and Connors, 2015; Pereyra et al., 2014). In the highly conserved p24 Gag region containing KK10, escape typically occurs via the sequential accumulation of two intraepitope mutations, L136M and R132K. The L136M substitution is thought to impair dendritic-cell-mediated antigen presentation by enhancing the interaction between HLA-B*27:05-KK10 and immunoglobulin-like transcript-4 (ILT-4) (Lichterfeld et al., 2007). This mutation also facilitates viral escape from initially mobilized clonotypes expressing public TCRs (Iglesias et al., 2011; Ladell et al., 2013). The R132K substitution abrogates peptide binding to HLA-B*27:05 (Goulder et al., 1997, 2001; Phillips et al., 1991). However, this mutation incurs a substantial fitness cost, which is partly counteracted by compensatory mutations elsewhere in p24 Gag (Ammaranond et al., 2005; Feeney et al., 2004; Goulder et al., 1997; Schneidewind et al., 2007, 2008, 2009). Epitopes restricted by other HLA class I allotypes overlap the KK10 region but are not associated with enhanced immune control, possibly because cytosolic nardilysin (NRDc) cleavage upstream of the ¹³¹KR¹³² motif destroys a subset of naturally generated peptides (Kessler et al., 2011).

Here, we investigated the impact of viral escape mutations in p24 Gag on antigen processing and transport and performed

structural and functional analyses of naturally produced KK10 epitope forms. Our findings revealed a mechanism of viral escape from CTL and NK responses based on antigen processing of different length variants of KK10 and peptide competition for binding to HLA-B*27:05. As HLA-B*27:05 confer substantial inherited risks to several autoimmune diseases, e.g., ankylosing spondylitis and acute anterior uveitis, our results indicate that peptide competition in this context might be used as a therapeutic approach to inhibit or silence errant immune responses.

RESULTS

CTL escape mutations distort proteasomal processing of KK10

Common KK10-associated CTL escape mutations (R132K and L136M) typically accumulate late in infection and are associated with sharp increases in viral replication (Feeney et al., 2004). However, the effects of these mutations on epitope processing have not been determined previously. As the HLA-B*27:05 allele is relatively frequent in white people, but rare in Black people (Gonzalez-Galarza et al., 2015), and the HIV-1 subtype B (HIV-B) predominates in white people (HIV Database, 2020) (Kist et al., 2020), we examined the impact of R132K and L136M on proteasomal processing of the KK10 epitope derived from HIV-B. Four 25-mer peptides were synthesized to match the consensus sequence of HIV-B (HIV Database, 2020), with or without one or both of the common escape substitutions: 25-KK10-wild type (WT), 25-KK10-R132 (K), 25-KK10-L136M (M), and 25-KK10-R132K/L136M (KM) (Figure 1A). We performed *in vitro* digestions of these 25-mer peptides using purified constitutive proteasomes and immunoproteasomes (containing subunits β 1i, β 2i, and β 5i) and analyzed the resulting fragments using mass spectrometry (Schmidt et al., 2012; Tenzer et al., 2009, 2014) (Figure 1A). KK10 epitope forms were defined as peptide fragments incorporating the R2 anchor and other segments of KK10. These peptide fragments could be extended by one or several residues at the N- and/or C terminus (Table S1) (Tenzer et al., 2009, 2014).

Constitutive proteasomal and immunoproteasomal digestion of the 25-KK10-WT peptide resulted in the production of KK10 and several epitope forms that were either truncated, including the KK10 minitopes (Tenzer et al., 2009) KRWI (K14), KRWII (K15), KRWIIL (KL6), KRWIILG (KG7), and KRWIILGL (KL8), or C-terminally extended, including KRWIILGLNKI (K11), KRWIILGLNKIVR (KR13), and KRWIILGLNKIVRM (KM14). The production of KK10 minitopes, especially KL6 and KL8, was favored by both proteasomal forms at all time points over the production of KK10 (Figure 1B). In contrast, only KK10 minitopes were generated from the singly substituted 25-mer peptides except for constitutive proteasomal digestion of the 25-KK10-K peptide, which produced small amounts of KK10-K (about 1.4% of all epitope forms) (Figures 1C and 1D; Table S1). Immunoproteasomal digestion of the 25-KK10-K peptide notably generated almost no KK10 epitope forms (<0.3% of all fragments). Constitutive and immunoproteasomal digestion of the doubly substituted 25-mer peptide again favored the production of

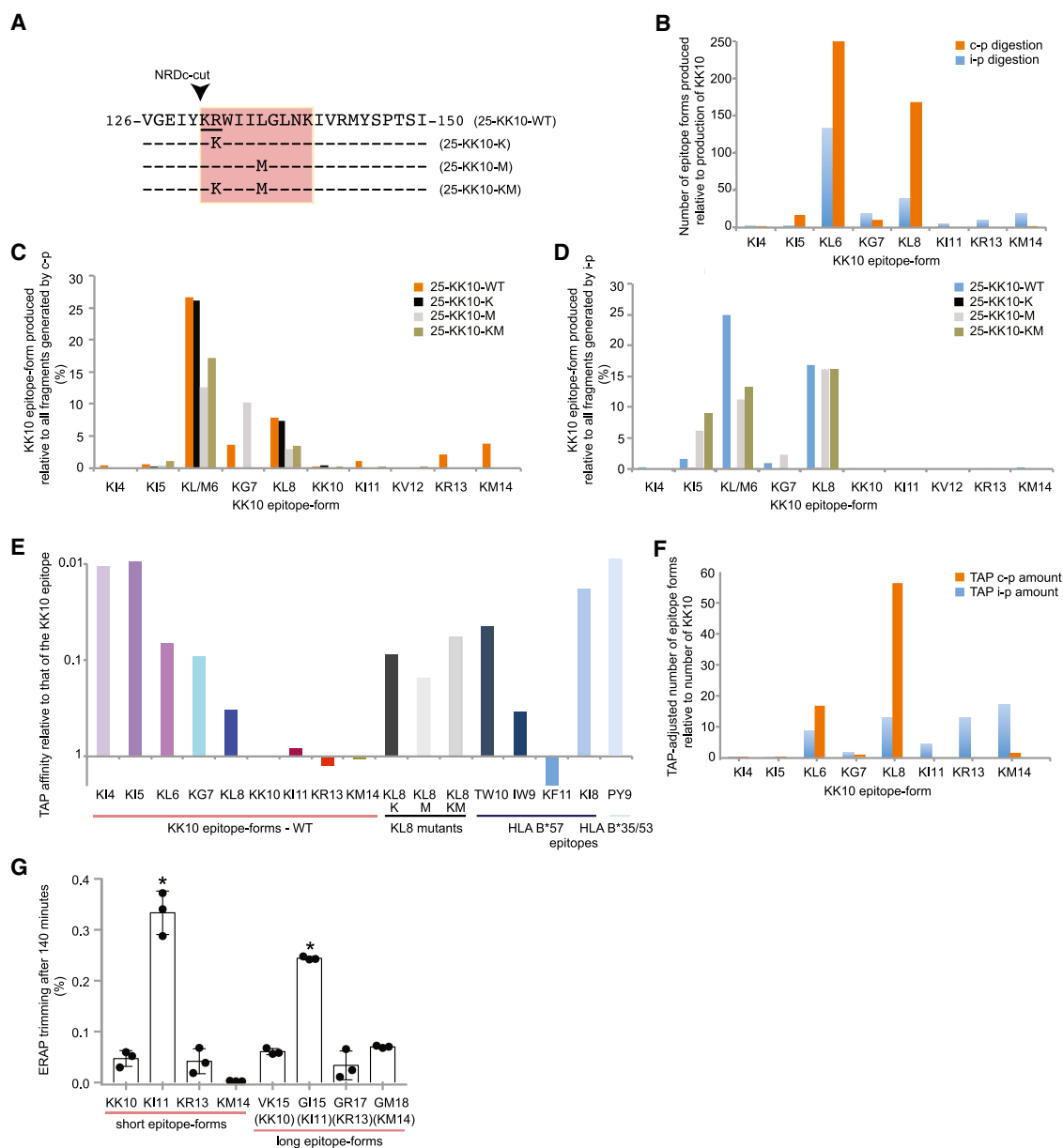


Figure 1. Antigen processing of the p24 Gag region incorporating KK10

(A) Outline of the p24 Gag region (amino acids 126–150). Alignments are shown for common escape mutations in the KK10 epitope (red). NRDc, cytosolic nardilysin. The NRDc recognition motif is underlined ($^{131}\text{KR}^{132}$).

(B) Production of KK10 epitope forms relative to the production of KK10 in proteasomal digests analyzed after 4 h to ensure full representation of all cleavage products (Tenzer et al., 2009, 2014).

(C and D) Percentage of KK10 epitope forms made after processing of 25-KK10-WT, 25-KK10-K, 25-KK10-M, or 25-KK10-KM by constitutive proteasomes (C) or immunoproteasomes (D). Proteasomal digests were analyzed after 4 h (Tenzer et al., 2009, 2014). KL/M6 indicates KL6 or KM6 epitope forms.

(E) Normalized TAP affinities for KK10 epitope forms relative to KK10. Comparative data are shown for TW10, IW9, KF11, KI8, and PY9, restricted by HLA-B*57:01/03 or HLA-B*35:01 (PY9 only) (HIV Database, 2020).

(F) TAP-adjusted production of KK10 epitope forms (details as in B).

(G) Percentage reduction in the abundance of KK10 and longer KK10 epitope forms after incubation with ERAP1/2 for 140 min (mean \pm SD).

See also Table S1. * $p < 0.0001$ (one-way ANOVA with Dunnett's test for multiple comparisons). KI11 was trimmed more than GI15 ($p = 0.0005$, Mann-Whitney U test). c-p, constitutive proteasome; i-p, immunoproteasome. Data are representative of 3–4 independent experiments (B–G).

KK10 minitopes but also generated some C-terminally-extended peptides, in total constituting 0.01% to 2.7% of all epitope forms (Figures 1C and 1D). However, epitope forms containing 132K cannot induce CTL responses because the R132K substitution thwarts KK10 binding to HLA-B*27:05 (Goulder et al., 2001; Phillips et al., 1991).

Proteasomal digestion of the 25-KK10-WT peptide therefore favored the production of KK10 minitopes with suboptimal HLA class I epitope lengths (Paul et al., 2013), and the presence of CTL escape mutations either skewed this preference further (R132K) or resulted in the exclusive production of KK10 minitopes (L136M).

Efficient binding of KK10 epitope forms to TAP

To induce a CTL response, the transporter associated with antigen processing (TAP) must transport processed KK10 epitope forms into the endoplasmic reticulum (ER). As TAP binding, not translocation, is the rate-limiting step (Gubler et al., 1998), we determined the normalized TAP affinities for all KK10 epitope forms. The results were adjusted to show epitope-form affinity relative to that of KK10 (Figure 1E).

TAP bound all KK10 epitope forms with a low-to-high affinity (Lauvau et al., 1999), which typically increased with epitope length. Even the binding of epitope forms with the lowest affinities (KI4 and KI5) was comparable to that of the immunodominant HLA-B*57:01/B*5703-restricted HIV-1 epitope KI8 (Goulder et al., 2000; Kloverpris et al., 2012) and the immunodominant HLA B*35:01-restricted HIV-1 epitope PY9 (Matthews et al., 2012). The affinities of KL6, KG7, and KL8 exceeded that of the immunodominant HLA-B*57:01/B*5703-restricted HIV-1 epitope TW10 (Goulder and Walker, 2012), and KL8 mutants bound TAP with intermediate affinity (Figure 1E).

Adjusting for TAP interactions changed the predicted relative abundance of epitope forms between the cytosol and the ER, such that KL8 became the dominant minitope, whereas KL6 was the most abundant epitope form after proteasomal digestion (Figures 1B and 1F). However, the overall predicted relative values for shorter and longer KK10 epitope forms in the ER still vastly exceeded that of KK10 (Figure 1F).

ERAP1/2 trimming is slow and maintains epitope diversity

After TAP-mediated transport into the ER, ER aminopeptidase (ERAP) might trim KK10 and the longer KK10 epitope forms, most likely before binding to HLA-B*27:05 (van Endert, 2011). To study this effect, we performed ERAP1/2 digestions (Tenzer et al., 2014) of N-terminally-extended epitope forms (Table S1) and epitope forms starting with ¹³¹K, equivalent to peptides that have undergone NRDC digestion (Figures 1A and 1G) (Kessler et al., 2011). We did not test truncated epitope forms because ERAP1 spares most peptides shorter than 8–9 amino acids (Chang et al., 2005; Saric et al., 2002; York et al., 2002). We observed only minimal ERAP1/2 trimming of most epitope forms (Figure 1G), but peptides ending with an I (KI11 and GI15) were trimmed significantly more than other epitope forms, and KI11 was trimmed faster than GI15. The specificity of ERAP1/2 was therefore likely insufficient to exert a marked effect on the relative abundance of KK10 epitope forms.

HLA-B*27:05 binds KK10 epitope forms

To examine if and how truncated and C-terminally-extended KK10 epitope forms bind HLA-B*27:05, we refolded epitope-form peptides with the HLA-B*27:05 heavy chain and β 2 microglobulin (β 2m). High-resolution crystal structures were obtained for HLA-B*27:05 in complex with three KK10 minitopes (KL6, KG7, and KL8) and three extended KK10 epitope forms (KI11, KR13, and KM14) (Table S2; Figure S1). However, we were unable to crystallize HLA-B*27:05-KI4 and HLA-B*27:05-KL5, despite the formation of heterotrimeric complexes that incorporated KI4 or KL5, respectively (Figure S2). To examine if ERAP1/2-digested peptides without the N-terminal R2_{peptide} bound to HLA-B*27:05, we set up refolds with the WIILGLNK (WK8) peptide. These refolds yielded no detectable heterotrimers (Figure S2D), suggesting that occupation of the C terminus alone was insufficient to stabilize HLA-B*27:05 (Xiao et al., 2017). As WK8 is not produced in KK10 digestions, we concluded that all naturally produced KK10 epitope forms bound HLA-B*27:05.

Three N-terminal amino acids are sufficient to stabilize HLA-B*27:05

We compared the seven KK10 epitope-form crystal structures to identify shared and distinct molecular features that might impact T and/or NK cell recognition. In each case, the N-terminal residue bound in the A pocket of HLA-B*27:05 (Figure S3), and the R2_{peptide} anchor docked in the B pocket, forming a network of hydrogen bonds and salt bridges with K1_{peptide}, E45_{B27}, and T24_{B27} (Figure 2A). The W3_{peptide} stacked against Y159_{B27} and L156_{B27} in the D pocket and interacted with W147_{B27} and V152_{B27} in the hydrophobic E pocket (Figures 2B and 2C). The I4_{peptide} occupied the C pocket and interacted with A69_{B27} and I66_{B27}. Collectively, these interactions resulted in a highly conserved structural motif that differed only in the KI11 structure (Figure 2D). In the KI11 structure, the C α of the I4_{peptide} was pushed upward and N-terminally compared with I4_{KK10} and did not interact with A69_{B27}. The associated normalized B factors were low, suggesting that this region was quite immobile (Figures 3A and 3B). This region also maintained a similar electrostatic surface potential throughout all structures unlike other regions, with the caveat of analytical limitations imposed by the bulging and truncated peptides (Figure S4).

Although residues 1 to 5 were in contact with the binding groove of HLA-B*27:05 in the KL6, KG7, and KL8 structures, residues 6, 7, and/or 8 were positioned above the groove and were solvent exposed (Figure 2D). The normalized B factors were very high for G7_{peptide} (in the KG7 and KL8 structures) and L8_{peptide} (in the KL8 structure) (Figures 3A and 3B), suggesting that these residues were mobile. In addition, the KL8 structure displayed weak electron density along the floor of the binding groove to the C terminus. This electron density pattern suggested the existence of a minority population (approximately 10%) of heterotrimeric complexes in which the peptide was “stretched” along the binding groove and bound at both the N- and C termini. Accordingly, the KL8 peptide might alternate between the extended “stretched-peptide” (KL8-SP) conformation and a more common partially bound conformation (Figures 2D, 3A, and S5). The lack of a C-terminal anchor in the KL6 and KG7 structures was associated with the outward displacement of the α 1_{B27} and α 2_{B27} helices, which

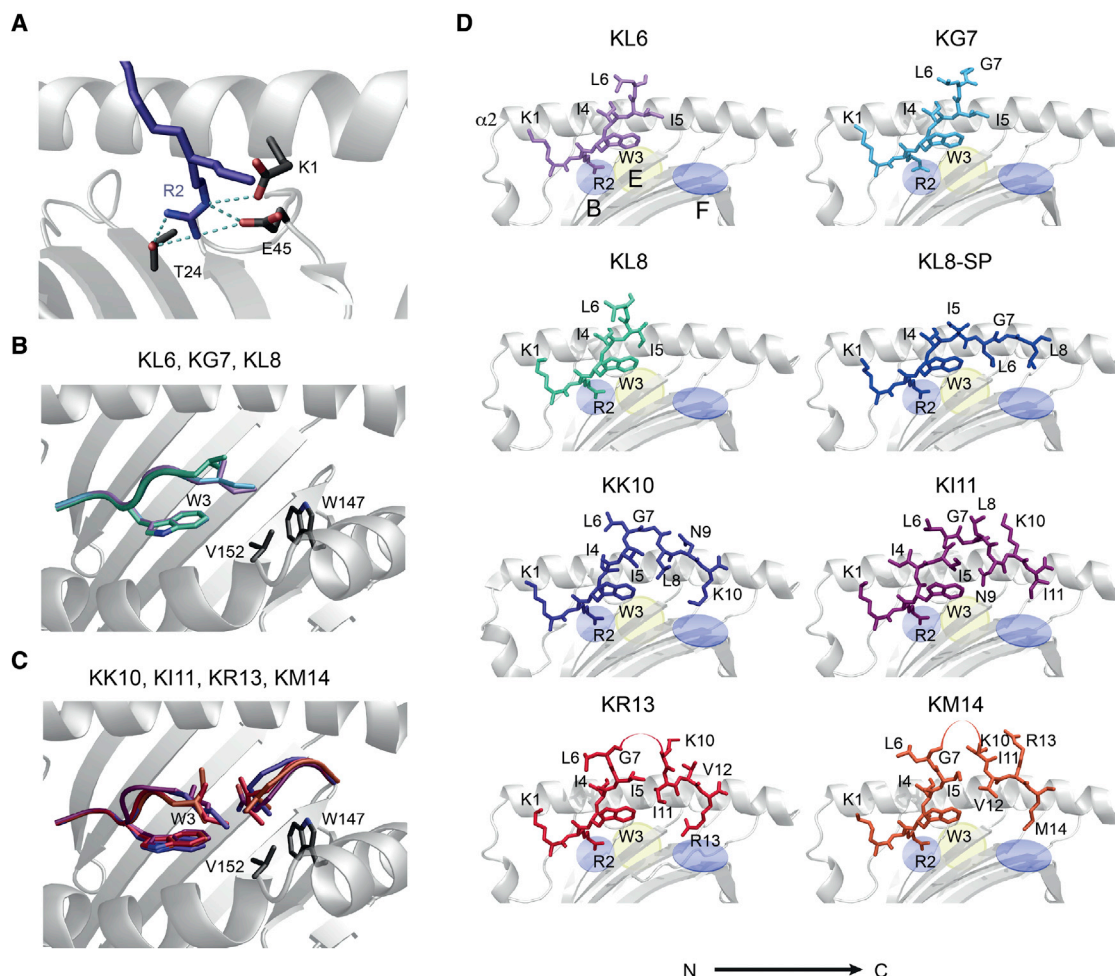


Figure 2. Shared N-terminal structural motif and side views of KK10 epitope forms complexed with HLA-B*27:05

(A) Model of the conserved N-terminal binding region in the HLA-B*27:05 groove. R2_{peptide} was stabilized via the formation of a planar hydrogen bond network between the E45_{B27} O_{E2} and the R2_{epitope} N_{H2} and N_E atoms and between the R2_{epitope} N_{H1} and N_{H2} atoms and the T24_{B27} O_Y atom.

(B and C) Model of W3_{peptide} interactions with W147_{B27} and V152_{B27} in the hydrophobic E pocket. These interactions were similar for truncated (B) and extended (C) KK10 epitope forms.

(D) Side views of the peptide-binding groove of HLA-B*27:05 complexed with KK10 epitope forms. The structure of HLA-B*27:05-KK10 was reported in [Stewart-Jones et al. \(2005a\)](#) (PDB: 2BSS). KK10 bound to the B- and F pockets of HLA-B*27:05 via anchors at positions 2 and 10 and formed a central peptide bulge (residues 4 and 7). Unmodeled central peptide residues with poor electron density are shown as a connecting arc. KL8 C-terminal unmodeled peptide residues are not shown. The KL8 structure appeared to have two conformations, with a minority population stretched along the floor of the binding groove (KL8-SP). Peptides are shown against the α 2_{B27} helix. The α 1_{B27} helix was removed for visual clarity. The B- and F pockets are indicated by light-blue disks and the E pocket by a light-yellow disk.

was greatest at the C-terminal end of the α 1_{B27} helix (0.92 Å) ([Figure S6](#)). A smaller displacement was observed in the KL8 structure, possibly because the KL8-SP conformation helped stabilize the α 1_{B27} and α 2_{B27} helices.

Collectively, these data revealed that the interaction between HLA-B*27:05 and the conserved, positively charged N-terminal KK10 region was sufficiently strong to stabilize the truncated peptide-HLA-B*27:05 complexes.

Differential binding of long KK10 epitope-form peptides to the E- and F pockets

The hydrophobic patch in the E pocket helped stabilize all epitope forms via interactions with W3_{peptide} ([Figures 2B and](#)

2C). This region also formed additional contacts with the longer epitope-form peptides. In the KK10, KR13, and KM14 structures, we observed shared hydrophobic interactions between V152_{B27} and the I5_{peptide} side chain and distinct interactions between V152_{B27} and L8_{peptide} in the KK10 structure ([Figure 4A](#)), I11_{peptide} in the KR13 structure, and V12_{peptide} in the KM14 structure ([Figure 4B](#)). In these structures, I5_{peptide} and the indicated hydrophobic residues were positioned at the N- and C-terminal ends of the central peptide loop, respectively, and the interaction of their side chains with each other and the E pocket potentially stabilized the central peptide loop ([Figure 4C](#)).

The KL8 and KI11 peptide interactions with the E pocket were different and appeared to be suboptimal. In the KL8 structure,

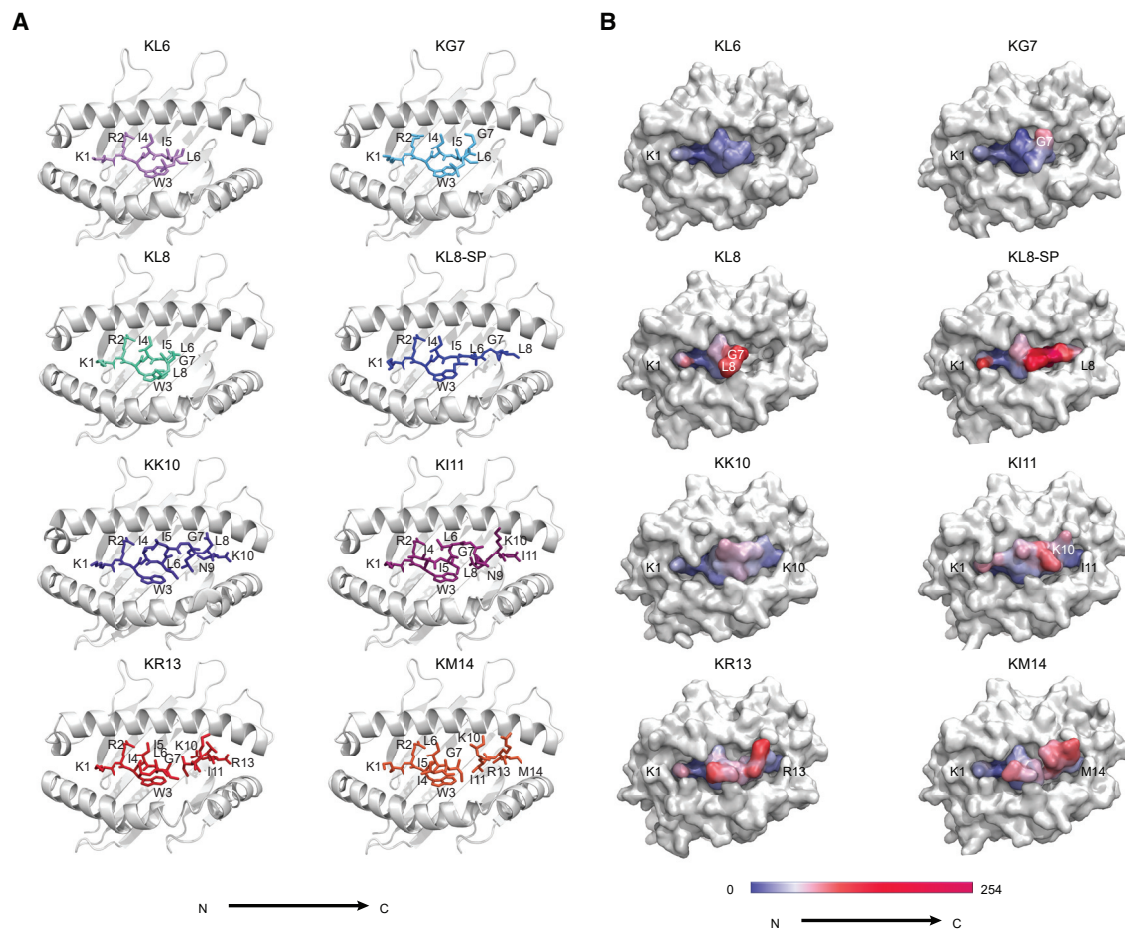


Figure 3. Top views of KK10 epitope forms complexed with HLA-B*27:05 and relative disorder of peptides

(A) Top views of the peptide-binding groove of HLA-B*27:05 complexed with KK10 epitope forms. The central peptide bulge in the KR13 and KM14 structures and the residues G7_{KL8} and L8_{KL8} were disordered.

(B) The relative local disorder of KK10 epitope-form peptides is derived from the normalized B factors associated with each structure in (A) after normalization of the B factors associated only with HLA-B*27:05 α -chain. Values represent local disorder of the peptide and are colored from blue (no disorder) to increasingly deeper shades of magenta (high disorder).

the I5_{peptide} side chain was rotated and perpendicular to the base of the groove, which increased the distance between the E pocket and the C δ 1 group to >5 Å (Figure 4D). In the KI11 structure, the C α of the I4_{peptide} and the C α of the I5_{peptide} were positioned above and more toward the N-terminal of the corresponding residues in the KK10 structure, which increased solvent exposure (Figures 4A and 4C). The position of L8_{peptide} was exceptional in the KI11 structure, as it formed part of the central loop (Figure 4C). Consequently, the hydrophilic N9_{peptide} side chain was directed toward the E pocket but kinked away, which allowed the δ -oxygen and δ -amino groups to interact with the ordered water molecules between the peptide and the α 1_{B27} helix (Figure 4C). This distinct arrangement of residues 4 to 9 resulted in a reduced interaction between I5_{peptide} and N9_{peptide} at the N- and C-terminal ends of the central peptide loop compared with that found in the KK10, KR13, and KM14 structures (Figures 4A and 4B) and a highly flexible K10_{peptide} that protruded by approximately 3 Å (Figures 3A and 4C). The distinct E-pocket

conformation and the larger central loop relative to KK10 also caused an exaggerated “zigzag” in the KI11 peptide backbone between the α 1_{B27} and α 2_{B27} helices, with marked tilting toward the α 2_{B27} helix compared with KK10 (Figures 4E and 4F). These features resulted in greater overall flexibility and solvent exposure of the central bulge compared with that of KK10, potentially giving rise to more recognition sites for TCRs.

The F pocket of HLA-B*27:05 binds a broader range of amino acids than other HLA-B*27 subtypes and most other HLA class I molecules (HIV Database, 2020). Hydrophobic residues at the entrance and acidic residues at the base allowed binding of either small hydrophobic side chains (L, I, and M in KL8, KI11, and KM14, respectively) or long basic side chains (K and R in KK10 and KR13, respectively). Although the different side chains interacted with distinct residues in the F pocket and carried different electrostatic charges, the peptide backbone conformations were remarkably similar (Figure 4E), and the B factors suggested that this region was relatively stable (Figure 3B). In the

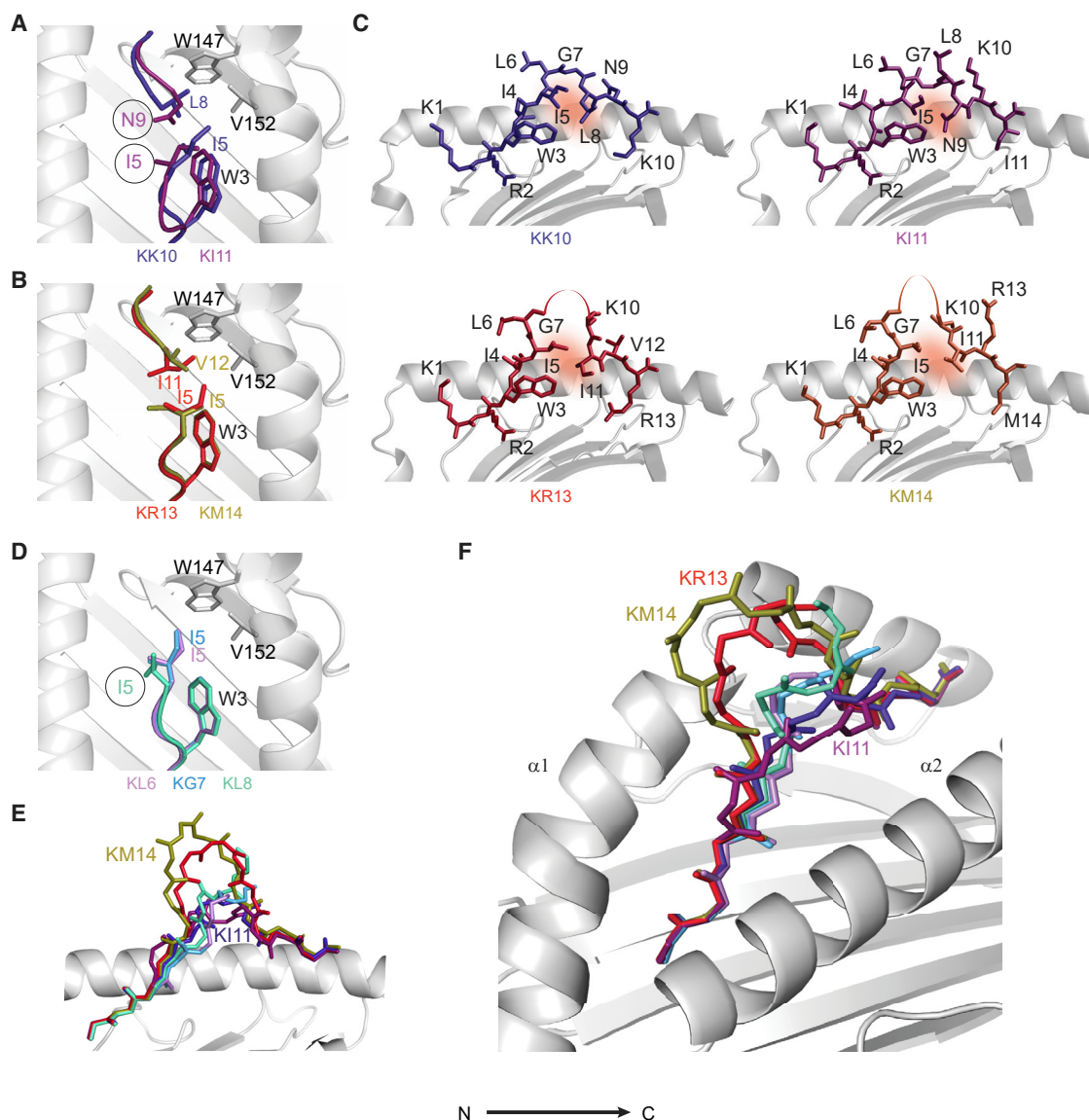


Figure 4. Shared and distinct binding motifs of KK10 epitope forms in the E- and F pockets of HLA-B*27:05

(A and B) Models show the partly distinctive way in which each KK10 epitope form interacted with the E pocket of HLA-B*27:05. Comparisons are shown for KK10 versus KI11 (A) and for KR13 versus KM14 (B). The distance between I5_{KI11} and V152_{B27} was 5 Å.

(C) Potentially stabilizing VDW interactions between the N- and C-terminal ends of the central peptide bulge in the KK10, KI11, KR13, and KM14 structures are shaded orange.

(D) As in (A) and (B) but comparing KL6, KG7, and KL8. The distance between I5_{KL8} and V152_{B27} was 7.1 Å, which precluded VDW interactions between the amino acid side chains.

(E and F) Overlay of all structures with peptide backbones shown (including unmodeled residues). The $\alpha 2_{B27}$ helix was removed from the side view (E) but not from the diagonal view (F). The positions of the central bulges in the longer KK10 epitope forms varied in distance from the $\alpha 2_{B27}$ helix: KI1 < KK10 < KM14 < KR13.

minitope structures, some electron density was present in the F pocket, and we identified an arginine in the KG7 structure that was most likely acquired from the refolding buffer and potentially helped stabilize HLA-B*27:05.

Collectively, these analyses revealed similar N- and C-terminal regions and distinct interactions with the E pocket and variable flexibility and solvent exposure in the central peptide loops of the longer epitope forms and further suggested that KL8 could

adopt multiple conformations in the binding groove of HLA-B*27:05.

Patterns of CTL recognition associate with patterns of viral escape

To examine the immunogenicity of naturally produced KK10 epitope forms, we used *ex vivo* interferon (IFN)- γ enzyme-linked immunospot (ELISpot) assays to quantify peptide-specific

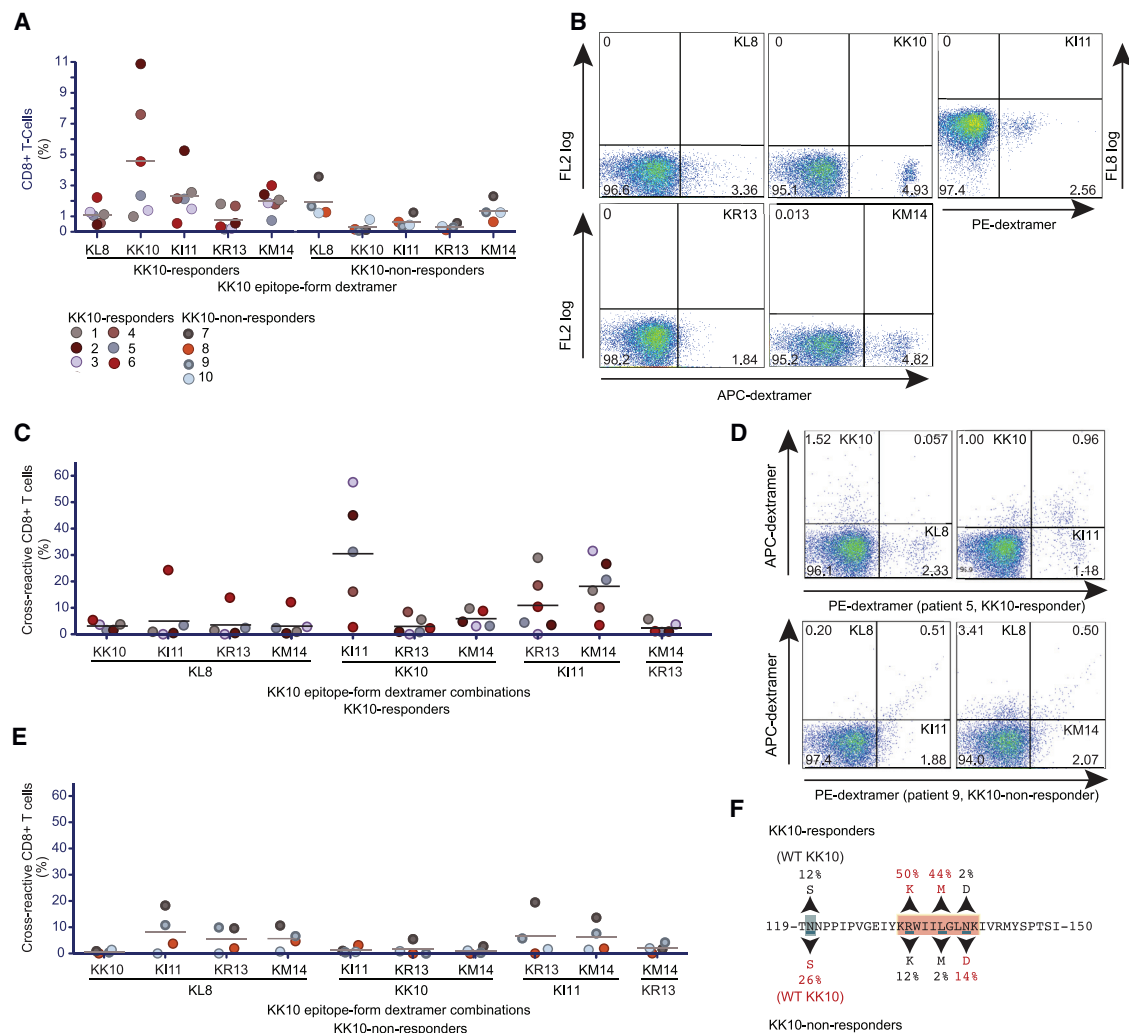


Figure 5. Ex vivo HLA-B*27:05-peptide dextramer reactivity and sequence variation in HIV-1

(A) Percentage of HLA-B*27:05-peptide dextramer⁺ CD8⁺ T cells in KK10 responders and KK10 non-responders. (B) Representative flow cytometry plots showing patterns of staining with individual HLA-B*27:05-peptide dextramers with dextramer fluorophore on the x axis (gated on viable CD3⁺ events). Numbers indicate quadrant percentages. (C) Percentage of cross-reactive CD8⁺ T cells in KK10 responders. (D) Representative flow cytometry plots showing cross-reactive staining with HLA-B*27:05-peptide dextramers (gated on viable CD3⁺ CD8⁺ events). Details as in (B). (E) Percentage of cross-reactive CD8⁺ T cells in KK10 non-responders. Details as in (C). (F) Proviral sequence variation in KK10 responders and KK10 non-responders. Common variants are highlighted in red. Horizontal bars indicate mean values (A, C, and E). Data are representative of at least 3 independent experiments (A–E).

responses among PBMCs isolated from ten HLA-B*27:05⁺ patients with chronic HIV-1 infection (Table S3) (Tenzer et al., 2009). Specific IFN- γ release was identified in response to KL8, KK10, KI11, KR13, and/or KM14 but not in response to other minitope peptides. The poor immunogenicity of KI4 and KI5 could be explained by poor or absent HLA-B*27:05 binding because these peptides refolded inefficiently *in vitro* with HLA-B*27:05. Similarly, the poor immunogenicity of KL6 and KG7 could be explained by the lack of C-terminal anchor residues and the associated outward displacement of the α_{1B27} and α_{2B27} helices, which might hinder productive TCR interactions.

To confirm these findings and assess cross-reactivity among epitope forms, we visualized antigen-specific CTLs directly *ex vivo* using HLA-B*27:05-peptide dextramers in conjunction with flow cytometry. KK10-specific CTL populations were observed in six patients (termed KK10 responders) and varied in magnitude from approximately 1%–11% of all CD8⁺ T cells (Figures 5A and 5B). CTL populations specific for other KK10 epitope forms were identified in the remaining four patients (KK10 non-responders) (Figures 5A and 5B). The biggest CTL populations in KK10 responders were directed against KK10, KI11, and KM14, and the biggest CTL responses in KK10 non-responders were directed against KL8 and KM14. These differences between

groups could be associated with distinct patterns of proteasomal digestion, as suggested previously (Tenzer et al., 2009, 2014) and by the data shown in Figure 1.

A similar pattern of flow cytometric dextramer staining was observed for each KK10 epitope form (Figure 5B). CTL populations identified with the KK10, KI11, and KM14 dextramers were typically discrete, whereas CTL populations identified with the KL8 and KR13 dextramers were usually less discrete (Figure 5B). Fluorescence intensity also varied with specificity. For example, the brightest stains were observed with the KK10 dextramer, whereas the most heterogeneous stains were observed with the KL8 and KR13 dextramers (Figure 5B). This latter observation suggests that CTL responses directed against KL8 and KM13 incorporated lymphocytes carrying TCRs with particularly diverse avidities compared with T cells recognizing KK10, KI11, and KM14 (Betts et al., 2004).

KI11-specific CTLs were more cross reactive than other epitope-form-specific CTLs (Figures 5C–5E). In KK10 responders, the mean cross-reactivity level was 16% of all KI11 dextramer⁺ cells, and in KK10 non-responders, it was 5.6% of all KI11 dextramer⁺ cells ($p = 0.032$, Mann-Whitney U test) (Figures 5C–5E). While KI11-specific CTLs among KK10 responders predominantly cross-recognized KK10 (Figure 5C), among KK10 non-responders, KI11-specific CTLs predominantly cross-recognized KL8 (Figure 5E). Other epitope-form-specific CTLs also predominantly cross-recognized KL8 in KK10 non-responders, suggesting a common mode of TCR engagement via the conserved N-terminal K₁R₂W₃ motif. In addition, KI11-specific CTLs in both patient groups frequently cross-recognized KR13 or KM14, but CTL cross-recognition between KR13 and KM14 was rare, suggesting that TCR docking sites were shared between KI11 and KR13 and between KI11 and KM14.

To evaluate the biological relevance of these observations, we isolated proviral DNA from KK10 responders and KK10 non-responders and sequenced the epitope-containing region of p24 Gag. The escape mutations R132K and L136M predominated in KK10 responders ($p < 0.0001$ for each mutation compared with KK10 non-responders, Fisher's exact test) (Figure 5F). In contrast, an upstream epitope-processing mutation (N120S) (Tenzer et al., 2014) predominated in KK10 non-responders ($p = 0.0486$ compared with KK10 responders, Fisher's exact test), invariably linked to the WT KK10 sequence (Figure 5F). The N120S substitution is a *bona fide* escape mutation because it abolishes the production of KL8, KK10, and KR13 (Tenzer et al., 2014). It may also impose structural constraints that impede the accumulation of intraepitope mutations, such as R132K and L136M.

Collectively, these results demonstrated a link between CTL specificity and the intrahost HIV-1 evolution.

Truncated KK10 epitope forms interfere with CTL recognition of KK10

Because KK10 minitopes were poorly immunogenic, we hypothesized that these epitope forms could compete for binding to HLA-B*27:05 in the ER. Such effects might limit the number of immunogenic KK10 epitope forms on the cell surface. To assess the functional consequences of epitope-form competition, we examined how CTL recognition of KK10 was affected by truncated epitope forms at relative concentrations similar to those generated by the proteasome (Figures 1B–1D).

generated by the proteasome (Figures 1B–1D).

In competition IFN- γ ELISpot assays (Figure 6A), a previously described KK10-specific CTL clone (G12C) (Ladell et al., 2013) became progressively less responsive at progressively higher concentrations of each truncated epitope form (Figure 6B). The inhibitory effects of KI4 and KI5 were less striking than those of the longer minitopes, likely reflecting lower binding affinities for HLA-B*27:05. Inhibition of the G12C response by a combination of minitopes was likewise more obvious in the presence of KL8 (Figure 6C). Comparison of these results with the processing data revealed that proteasomal digestion produced enough KL6 and KL8 to more than halve the G12C response to KK10 and enough KL6 and KL8 in combination with other epitope forms to inhibit the G12C response to KK10 by $\geq 70\%$ (Figures 6B and 6C). In contrast, the G12C response was enhanced in a concentration-dependent manner by the addition of KR13 or KM14, and these responses were inhibited by the addition of KK10, suggesting preferential recognition of the longer epitope forms (Figure S7).

In competition intracellular cytokine staining (ICS) assays performed directly *ex vivo* (Figure 6D), a combination of KI4, KI5, KL6, and KG7 inhibited the KK10-specific CTL response less than a combination of KI4, KI5, KL6, KG7, and KL8 (Figure 6E). These inhibitory effects were observed across different effector functions, including the mobilization of CD107a and the production of IFN- γ and TNF- α , and were consistent with the G12C data (Figure 6C).

Collectively, these results demonstrated that truncated KK10 epitope forms, and particularly the longer minitopes, were able to compete for binding to HLA-B*27:05 and inhibit CTL responses to KK10 and its extended epitope forms *in vitro*, consistent with a previously unrecognized mechanism of viral escape *in vivo*.

KIR3DL1 binding and the effect of mutations depend on KK10 epitope form

Binding of the inhibitory KIR receptor, KIR3DL1, to HLA-B*27:05-KK10 is associated with a weak but consistently beneficial effect on immune control of HIV-1, while binding to HLA-B*57:01 confers more robust control (Boelen et al., 2018; Martin and Carington, 2013; Martin et al., 2007; Stewart-Jones et al., 2005a). Previous work has shown that KIR3DL1 binds HLA-B*27:05-peptide complexes with a footprint that includes residues 77_{B27}, 81_{B27}, 84_{B27}, and 88_{B27} and the C terminus of the peptide, including the amino acid residues at positions 7 (or C-2) and 8 (or C-1) (Peruzzi et al., 1996; Stewart-Jones et al., 2005a). This binding mode suggests that direct interactions are unlikely between KIR3DL1 and HLA-B*27:05 in complex with KI4, KI5, KL6, or KG7. However, these truncated epitope forms might indirectly limit interactions with KIR3DL1 by outcompeting longer epitope forms for binding to HLA-B*27:05.

We measured KIR3DL1 binding to KK10 epitope forms complexed with HLA-B*27:05 using the corresponding dextramers and a BAF cell line stably transfected with KIR3DL1*001 (Stewart-Jones et al., 2005a) (Figure 7A). Similar experiments were performed using HLA-B*57:01 and HLA-B*57:03 dextramers complexed with the p24 Gag epitopes IW9 or KF11 to quantify protective KIR3DL1 interactions associated with elite control of

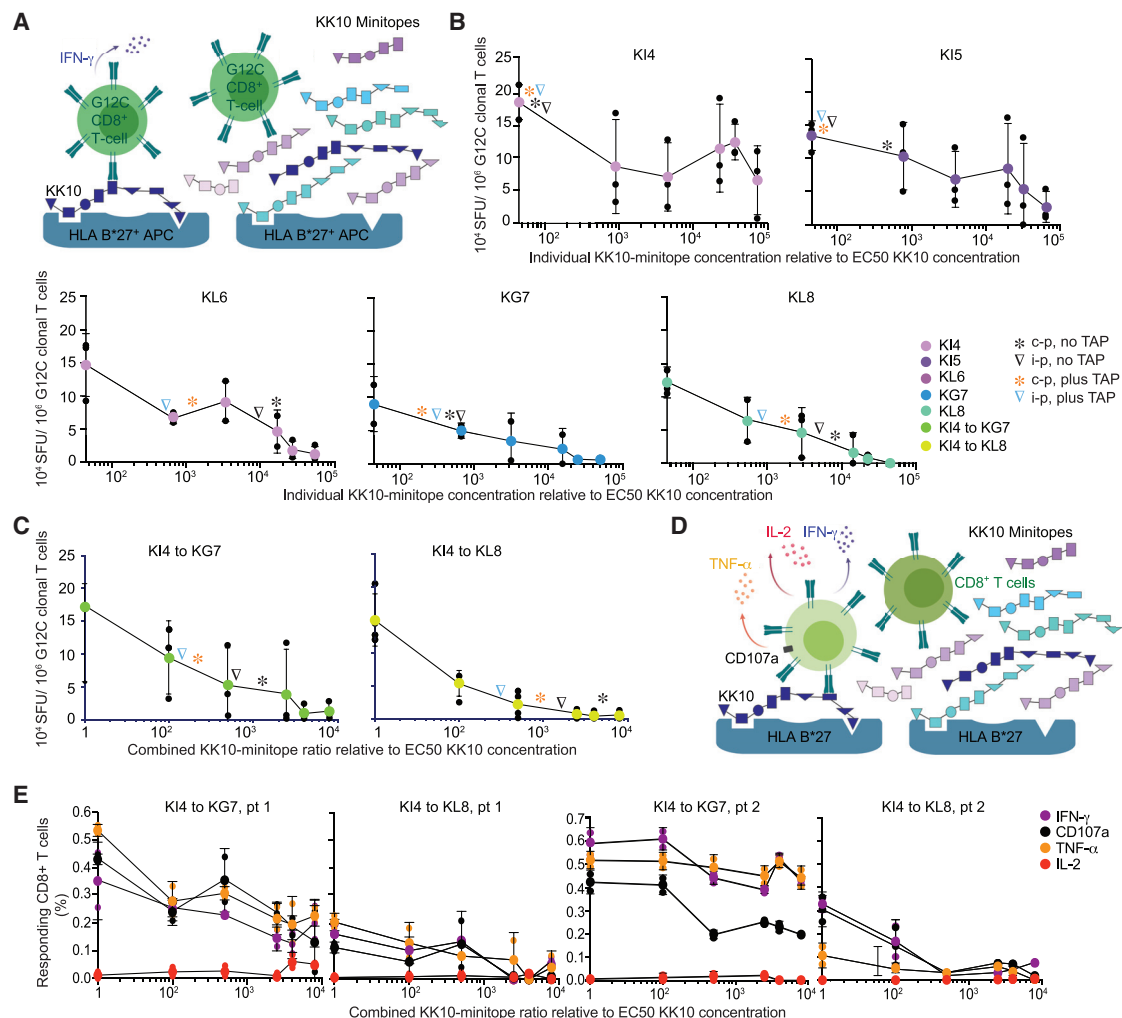


Figure 6. Inhibitory effects of KK10 minitopes on the functional reactivity of KK10-specific CTLs

(A) Outline of the IFN- γ ELISpot competition experiment with the KK10-specific CTL clone G12C and Tap-deficient HLA-B*27:05-transfected antigen-presenting cells (APCs).

(B) IFN- γ release by G12C in response to KK10 at the half maximal effective concentration (EC_{50}) molar concentration in the presence of individual KK10 minitopes at molar ratios of 1, 10, 50, 250, 400, and 800 relative to KK10. The corresponding molar ratios after processing (4 h) by constitutive proteasomes (c-p) or immunoproteasomes (i-p) are indicated by asterisks or inverted triangles, respectively. Non-TAP-adjusted ratios are shown in black. TAP-adjusted ratios are shown in orange (c-p) or blue (i-p). ELISpot data are shown as spot-forming units (SFUs) per 10^6 cells. Data were concatenated from 3 independent experiments (black dots). Colored dots indicate mean values. Error bars indicate SD.

(C) IFN- γ release by G12C in response to KK10 at the EC_{50} molar concentration in the presence of multiple KK10 minitopes at molar ratios of 1, 10, 50, 250, 400, and 800 relative to KK10. Details as in (B).

(D) Outline of the intracellular cytokine staining (ICS) competition experiment with CD8 $^{+}$ T cells from HLA-B*27:05 $^{+}$ patients.

(E) Mobilization of CD107a (black) and production of IFN- γ (purple), TNF- α (orange), and interleukin (IL)-2 (red) by CD8 $^{+}$ T cells in response to KK10 at the EC_{50} molar concentration in the presence of multiple KK10 minitopes at molar ratios of 1, 10, 50, 250, 400, and 800 relative to KK10. Each function was measured by flow cytometry as a percentage of the total CD8 $^{+}$ T cell population. Data were concatenated from 3 or 4 independent experiments (black dots). Colored dots indicate mean values. Error bars indicate SD.

HIV-1 (Carrington and Alter, 2012; Song et al., 2014) (Figure 7B). As expected, KIR3DL1 bound strongly to HLA-B*57:01/03, especially in complex with IW9 (Figure 7B). In contrast, a substantially weaker interaction was observed between KIR3DL1 and HLA-B*27:05-KK10 (Figure 7B).

The interaction between KIR3DL1 and HLA-B*27:05-KI11 was approximately 50% weaker in terms of fluorescence intensity

than the interaction between KIR3DL1 and HLA-B*27:05-KK10 (Figure 7A). Further reductions were observed with other epitope forms (KM14 > KL8 > KR13) (Figure 7A). These results might be explained by the unstable conformation of KL8 and steric interference arising from the central peptide bulges in KR13 and KM14. Incorporation of the L136M mutation into KL8 marginally increased binding to KIR3DL1. *In silico* modeling suggested that

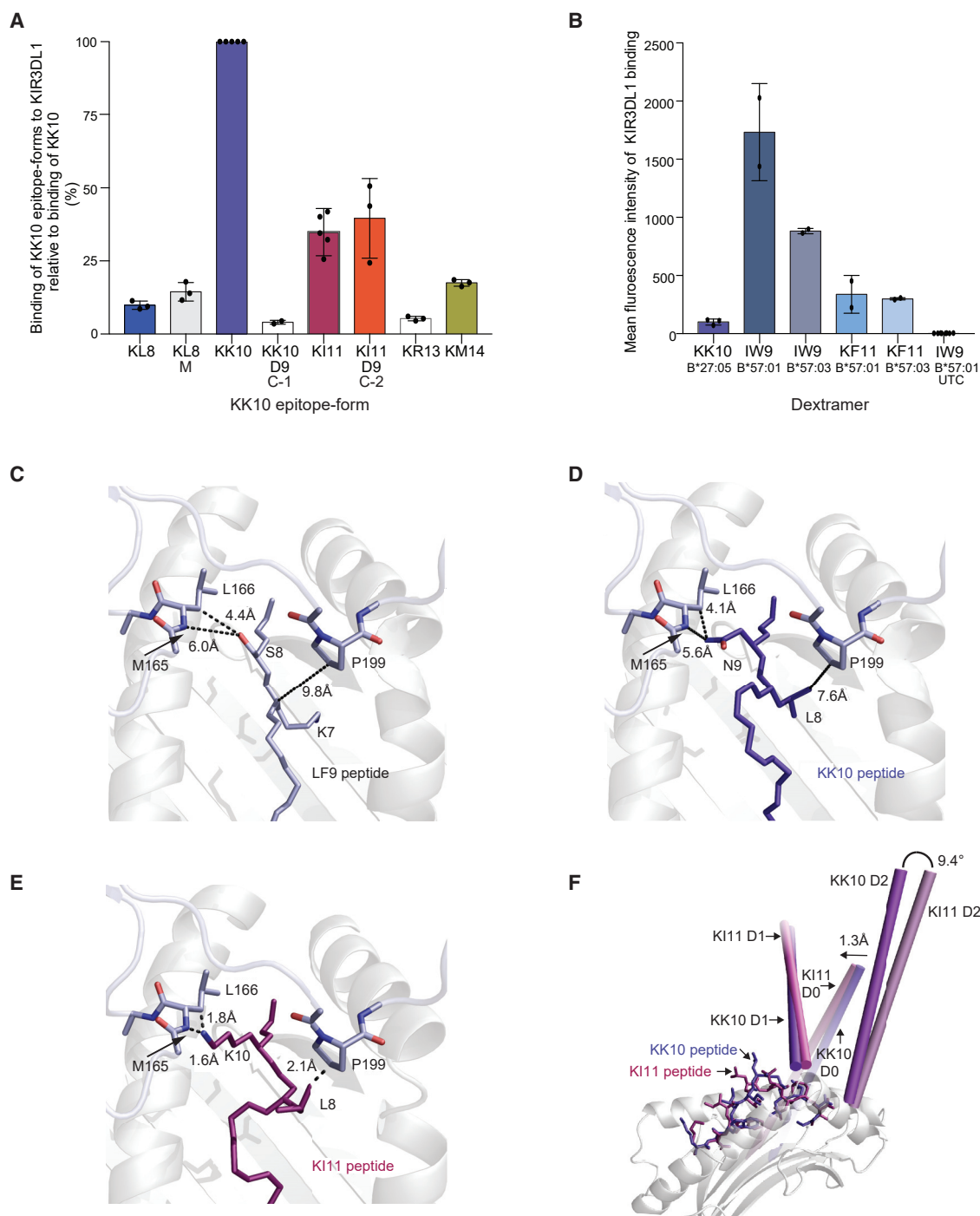


Figure 7. KIR3DL1 binding to KK10 epitope forms complexed with HLA-B*27:05 and modeling of KIR3DL1 interactions

(A) HLA-B*27:05-peptide dextramer staining of a BAF cell line stably transfected with KIR3DL1*001. Percentages are shown relative to KK10. The L136M mutation favored the production of KK10 minitopes and was therefore only tested in the KL8 epitope form (KL8-M). KIR3DL1 binding was reduced for all epitope forms relative to KK10 ($p < 0.0001$, one-way ANOVA with Dunnett's test for multiple comparisons).

(B) Mean fluorescence intensity of KIR3DL1 binding to HLA-B*27:05-KK10 and HLA-B*57:01-IW9, HLA-B*57:03-IW9, HLA-B*57:01-KF11, and HLA-B*57:03-KF11. KIR3DL1 binding was reduced for HLA-B*27:05-KK10 relative to all other dexamers ($p < 0.001$ one-way ANOVA with Dunnett's test for multiple comparisons). Black dots represent independent experiments.

(A and B) Error bars indicate SD.

(C) Interaction between KIR3DL1 and the LF9 peptide in the 3VH8-HLA-B*57:01 complex (Vivian et al., 2011) (PDB: 3VH8) showing a VDW contact between S8_{peptide} and L166_{KIR3DL1} (dotted line, 4.4 Å). This residue also had a water-mediated interaction with KIR3DL1.

(legend continued on next page)

KIR3DL1 docked onto HLA-B*27:05-KK10 in a manner similar to the reported interaction with HLA-B*57:01-3VH8 (Vivian et al., 2011) (Figures 7C and 7D), whereas the interaction with HLA-B*27:05-KI11 likely would be hampered by the protruding K10_{KI11} (Figure 7E). The model suggested that the protruding K10_{KI11} would alter the position of the D1 domain, leading to shifts in all three KIR domains that would change and/or disrupt contacts across the interface (Figure 7F).

The N139D mutation predominated in KK10 non-responders (Figure 5F). To examine the effect of this substitution on KIR3DL1 recognition, we measured KIR3DL1 binding using HLA-B*27:05 dextramers complexed with KK10-D9 (C-1) or KI11-D9 (C-2). The D9 substitution in KK10 dramatically reduced binding to KIR3DL1 (Figure 7A), and modeling suggested that the negatively charged D9_{peptide} disrupted hydrogen bonds between N9_{KK10} and E76_{B27} and N77_{B27} in the α 1_{B27} helix. The presence of a negative charge at the C-1 position has been shown previously to abolish KIR3DL1 recognition (Brackenridge et al., 2011; O'Connor et al., 2015). In contrast, KIR3DL1 bound equivalently to HLA-B*27:05-KI11 and HLA-B*27:05-KI11-D9 (Figure 7A). This experimental observation and modeling suggested that the D9_{peptide} side chain adopted a similar conformation to the N9_{KI11} side chain, which pointed toward the binding groove of HLA-B*27:05 (Figure 4A). Alternatively, the D9 substitution induced subtle changes in peptide conformation, which differed in the context of KK10 and KI11 (Iversen et al., 2006).

Collectively, these findings showed that KIR3DL1 bound less avidly to HLA-B*27:05 complexed with any KK10 epitope form than to HLA-B*57:01/03 complexed with IW9 or KF11. Moreover, KIR3DL1 bound less well to all immunogenic non-10-mer KK10 epitope forms than to the optimal KK10 epitope form. Notably, if the intraepitope N139D mutation was present in the KK10 epitope, the binding to KIR3DL1 was markedly reduced, whereas no significant reduction was observed when the mutation was present in the KI11 epitope form. Together, the processing of multiple epitope forms and intraepitope mutations resulted in a relative decrease in the binding strength between KIR3DL1 and the HLA-B*27:05-peptide complex, which likely decreases inhibitory KIR signaling and the NK response to HIV-1 infection (Boudreau et al., 2016; Saunders et al., 2016). These results are consistent with the absent/weak and strong biological effects of inhibitory KIR interactions with HLA-B*27:05 and HLA-B*57:01/03, respectively, in HIV-1 containment (Martin and Carrington, 2013; Martin et al., 2007).

DISCUSSION

Here, we found that the immunodominant KK10 region of p24 Gag was naturally processed into multiple epitope forms, many

of which bound TAP and HLA-B*27:05. Structural analyses revealed distinct and shared molecular features that affected immune recognition of these epitope forms via KIR3DL1 and TCRs. In addition, common intraepitope CTL escape mutations, including R132K (Feeney et al., 2004; Goulder et al., 1997) and L136M (Almeida et al., 2007; Ammaranond et al., 2005; Feeney et al., 2004; Goulder et al., 1997; Ladell et al., 2013; Schneidewind et al., 2007, 2008), skewed proteasomal activity to favor the production of KK10 minitopes, which competitively limited interactions with KIR3DL1 and TCRs. Even very short minitopes, such as KI4 and KI5, incorporated optimal amino acids that allowed for binding to TAP (Momburg et al., 1994a, 1994b; van Endert, 2011; van Endert et al., 1995). However, although TAP binding is the rate-limiting step, translocation into the ER of such short peptides has not been proved nor disproved experimentally (Gubler et al., 1998). Processing of multiple epitope forms, including the generation of inhibitory minitopes, was therefore identified as a mechanism of viral escape from CTL responses and inhibitory KIR binding in the context of the protective allotype HLA-B*27:05.

In patients with KK10-specific CTL responses, the intraepitope substitutions R132K and L136M predominated at the level of proviral DNA. These mutations are known to impose fitness costs on HIV-1 (Schneidewind et al., 2008). A KK10-specific CTL selection pressure was therefore apparent in these patients, despite the relatively low amount of KK10 produced following processing of the HIV-1 subtype B WT sequence. This observation could be explained by the fact that very few cell surface recognition events are required to activate CTLs (Purbhoo et al., 2004). That the intraepitope CTL escape mutation, L136M, skewed processing toward exclusive production of KK10 minitopes would further aid viral escape and might help explain why cross-reactive CTLs ultimately fail to prevent disease progression in HLA-B*27:05⁺ individuals with enhanced immune control of HIV-1 (Ladell et al., 2013). The R132K mutation abrogated binding to HLA-B*27:05, which resulted in viral escape regardless of epitope form. In patients without a KK10-specific CTL response, the extraepitope substitution N120S predominated at the level of proviral DNA. This mutation was invariably associated with an intact KK10 sequence and likely disrupted the production of multiple epitope forms to prevent immune recognition by cross-reactive or variant-specific TCRs (Tenzer et al., 2014).

KIR3DL1 bound less well to HLA-B*27:05 complexed with KK10 than to HLA-B*57:01/03 complexed with the protective epitopes IW9 or KF11, and binding decreased further when considering shorter or longer KK10 peptide variants. Strong inhibitory KIR3DL1 ligation has been demonstrated to improve NK cell activation and antibody-dependent cellular cytotoxicity

(D) *In silico* modeling of the KIR3DL1 interaction with HLA-B*27:05-KK10 using LSQ alignment of C α atoms from residues 1–180 of HLA-B*27:05. The image shows that a VDW contact could be formed between N9_{KK10} and L166_{KIR3DL1} (dotted line, 4.1 Å).

(E) *In silico* modeling of the KIR3DL1 interaction with HLA-B*27:05-KI11 as in (D). The protruding K10_{KI11} might interact with E282_{KIR3DL1} and/or form a VDW contact with L166_{KIR3DL1} (dotted line, 1.8 Å) and/or a hydrogen bond contact with M165_{KIR3DL1} (dotted line, 1.6 Å). This protrusion could “push” KIR3DL1 away and/or disrupt the ordered water molecules between KIR3DL1 and HLA-B*27:05.

(F) *In silico* modeling of the shift in the KIR3DL1 D0, D1, and D2 domains after binding to HLA-B*27:05-KK10 (blue purple) or HLA-B*27:05-KI11 (red purple). The largest shift was 1.3 Å in the D1 domain, and the position of KIR3DL1 was altered by up to 9.4° in the D0 domain. The KIR3DL1 domains are represented by sticks. Models were generated using HADDOCK.

(ADCC), inhibit HIV-1 replication in autologous infected CD4+ T cells, and enhance survival of CD8+ T cells in viral infection (Boelen et al., 2018; Boudreau et al., 2016; Song et al., 2014). The HIV-1 Nef protein selectively downregulates HLA-A and -B, which aid viral escape from the CTL response but render the cells vulnerable to NK lysis. Differential epitope peptide processing, and the competition between immunogenic and non-immunogenic epitope forms within the ER, would likely decrease inhibitory KIR3DL1 signaling in HIV-infected patients with HLA-B*27:05 and might therefore provide a viral escape mechanism.

The effect of the intraepitope mutation (N139D) on KIR3DL1 binding differed considerably depending on the length of the epitope form containing the mutation as binding was reduced in the context of KK10 and unaffected in KI11. As far as we know, this phenomenon has not been previously reported and underscores that epitope-processing patterns need to be considered when assessing the effects of mutations on binding to KIR3DL1.

The epitope form KI11 was frequently cross recognized in patients with or without a contemporaneous response to KK10. This observation could be explained by the conserved N- and C-terminal motifs and the distinct central peptide bulge in HLA-B*27:05-KI11. The latter appeared more stable than the corresponding peptide bulges in HLA-B*27:05-KR13 and HLA-B*27:05-KM14, potentially enabling more productive interactions with cross-reactive TCRs. Comparable peptide bulges have been observed previously in complexes with other HLA class I allotypes (Hillig et al., 2004) (Stewart-Jones et al., 2005b) (Tynan et al., 2005) (Probst-Kepper et al., 2004) (Bade-Doding et al., 2011).

The poor definition and variable fluorescence of KL8-specific CTL populations suggested cross-recognition via an array of clonotypes, potentially reflecting the availability of distinct structural features in the antigenic complex, such as the conserved N-terminal K₁R₂W₃ motif and the exposed C-terminal residues in the partially bound conformation, which might be forced into the less common extended conformation after engagement with particular TCRs. This interpretation contrasted with the single recognition structure model (Bordner, 2010) and was somewhat analogous to earlier observations in the murine I-E^k system (Schmitt et al., 1998).

Peptide competition has been mooted as a therapeutic approach to inhibit or silence errant immune responses in autoimmunity (Lock et al., 1991). Our results provide an indirect proof of concept that such a strategy could work *in vivo* because the production of inhibitory peptides was favored as a means of viral escape by natural selection. HLA-B*27:05 confers a strong inherited risk to several autoimmune diseases, e.g., ankylosing spondylitis, juvenile arthritis, reactive arthritis, and acute anterior uveitis. Although treatment of these diseases has been revolutionized with the advent of tumor necrosis factor (TNF) inhibitors, many patients do not respond or show loss of clinical response over time. Therefore, new therapeutic modalities are needed. Our study indicates that it might be possible to design inhibitory peptides, or perhaps short versions of key disease-associated peptides, that bind with high affinity to the HLA-B*27:05 peptide-binding cleft and hamper pathogenic T cell responses. Innovative vehicles might be required to deliver such peptides to

disease sites, e.g., exosomes (Barile and Vassalli, 2017), although recent immunotherapy with peptides designed to bind the HLA binding cleft to modify type 1 diabetes causing T responses showed promise following intravenous administration (Alhadj Ali et al., 2017).

It will be important to confirm and extend the findings reported here across other antigenic regions of HIV-1 and possibly other viruses. As the epitope-specific CTL response is influenced by the abundance (Schmidt et al., 2012; Tenzer et al. 2009, 2014) and length of the specific epitope peptide (Iversen et al., 2006), it will likely be possible to use the knowledge gained from antigen-processing analyses of HIV-1 to “reverse engineer” and create artificial HIV-1 vaccine inserts that increase the processing of specific, highly immunogenic forms of selected epitopes.

Limitations of the study

We determined the TAP affinities of the KK10 epitope peptides, as TAP binding is the rate-limiting step for peptide transport into the ER (Gubler et al., 1998). However, it cannot be ruled out that translocation efficiency might differ. The current peptide elution technology prevented simultaneous analyses of the peptide repertoire in the ER and the cell surface. As a result, the intracellular competition between the peptides had to be analyzed through peptide competition experiments at the cell surface.

STAR★METHODS

Detailed methods are provided in the online version of this paper and include the following:

- **KEY RESOURCES TABLE**
- **RESOURCE AVAILABILITY**
 - Lead contact
 - Materials availability
 - Data and code availability
- **EXPERIMENTAL MODELS AND SUBJECT DETAILS**
 - Patients and HLA genotyping
- **METHOD DETAILS**
 - Peptide synthesis and purification
 - Proteasome purification and *in vitro* digestions
 - Analysis of peptide digests by mass spectrometry
 - TAP-peptide binding assays and ERAP1/2 digestions
 - Expression, purification, and crystallization of HLA-B*27:05-peptide complexes
 - Modeling of HLA-B*27:05-peptide complexes and the interaction between HLA-B*27:05 and KIR3DL1*001
 - *Ex vivo* staining of PBMCs with HLA-B*27:05-peptide dextramers
 - Amplification and sequencing of HIV-1 p24 Gag
 - Standard and competition IFN- γ ELISpot assays
 - Standard and competition ICS assays
 - KIR3DL1*001 binding assay
- **QUANTIFICATION AND STATISTICAL ANALYSIS**

SUPPLEMENTAL INFORMATION

Supplemental information can be found online at <https://doi.org/10.1016/j.celrep.2022.110449>.

ACKNOWLEDGMENTS

We thank the patients for donating samples, Bente Baadegaard and Lene Pors Jensen for patient management, Dorthe Hass for expert technical assistance, E. Yvonne Jones for access to facilities, support, and helpful discussions, and Jamie Rossjohn for helpful discussions. This work was supported by the Medical Research Fund at Oxford University (HM1090) (A.K.N.I.), the Oak Foundation (OFIL-20-095) (A.K.N.I.), the Genomes2Vaccines (STREP), FP6, contract number LSHB-CT-2003-503231 (P.v.E.), the Hochschulbau-förderungsgesetz Program (HBFG-122-605) (S.T. and H.S.), the German Research Foundation (CRC 1292, TP13, and Z01) and the Forschungszentrum für Immuntherapie (FZI) Mainz (S.T. and H.S.). D.A.P. is a Wellcome Trust Senior Investigator (100326/Z/12/Z).

AUTHOR CONTRIBUTIONS

A.K.N.I. conceived, designed, and managed the study; P.P., S.T., E.W., M.W., A.B., S.K., M.H., and A.K.N.I. performed experiments; S.T., H.S., P.v.E., M.H., and A.K.N.I. planned and supervised experiments; P.P., S.T., P.v.E., M.H., and A.K.N.I. analyzed data; P.P., T.M.J., and M.H. performed structural modeling; J.G. and A.K.N.I. provided patient samples; K.L., J.E.M., V.A., D.A.P., L.F., J.I.B., H.S., P.v.E., and A.K.N.I. provided reagents; A.K.N.I. and P.P. wrote the manuscript; D.A.P., P.v.E., and M.H. provided intellectual input; and A.K.N.I. and D.A.P. edited the final manuscript. All authors commented on the manuscript prior to submission.

DECLARATION OF INTERESTS

The authors declare no competing interests.

Received: April 23, 2020

Revised: October 31, 2021

Accepted: February 7, 2022

Published: March 1, 2022

REFERENCES

- Adams, P.D., Afonine, P.V., Bunkoczi, G., Chen, V.B., Davis, I.W., Echols, N., Headd, J.J., Hung, L.W., Kapral, G.J., Grosse-Kunstleve, R.W., et al. (2010). PHENIX: a comprehensive Python-based system for macromolecular structure solution. *Acta Crystallogr. Section D, Biol. Crystallogr.* **66**, 213–221.
- Alhadij Ali, M., Liu, Y.F., Arif, S., Tatovic, D., Shariff, H., Gibson, V.B., Yusuf, N., Baptista, R., Eichmann, M., Petrov, N., et al. (2017). Metabolic and immune effects of immunotherapy with proinsulin peptide in human new-onset type 1 diabetes. *Sci. translational Med.* **9**, eaaf7779.
- Almeida, J.R., Price, D.A., Papagno, L., Arkoub, Z.A., Sauce, D., Bornstein, E., Asher, T.E., Samri, A., Schnuriger, A., Theodorou, I., et al. (2007). Superior control of HIV-1 replication by CD8+ T cells is reflected by their avidity, polyfunctionality, and clonal turnover. *J. Exp. Med.* **204**, 2473–2485.
- Altfield, M.A., Trocha, A., Eldridge, R.L., Rosenberg, E.S., Phillips, M.N., Addo, M.M., Sekaly, R.P., Kalams, S.A., Burchett, S.A., McIntosh, K., et al. (2000). Identification of dominant optimal HLA-B60- and HLA-B61-restricted cytotoxic T-lymphocyte (CTL) epitopes: rapid characterization of CTL responses by enzyme-linked immunospot assay. *J. Virol.* **74**, 8541–8549.
- Ammananond, P., Saunders, J., Satchell, C., van Bockel, D., Cooper, D.A., and Kelleher, A.D. (2005). A new variant cytotoxic T lymphocyte escape mutation in HLA-B27-positive individuals infected with HIV type 1. *AIDS Res. Hum. retroviruses* **21**, 395–397.
- Bade-Dodging, C., Theodossis, A., Gras, S., Kjer-Nielsen, L., Eiz-Vesper, B., Seltsam, A., Huyton, T., Rossjohn, J., McCluskey, J., and Blaszczyk, R. (2011). The impact of human leukocyte antigen (HLA) micropolymorphism on ligand specificity within the HLA-B*41 allotypic family. *Haematologica* **96**, 110–118.
- Baker, N.A., Sept, D., Joseph, S., Holst, M.J., and McCammon, J.A. (2001). Electrostatics of nanosystems: application to microtubules and the ribosome. *Proc. Natl. Acad. Sci. U S A* **98**, 10037–10041.
- Barile, L., and Vassalli, G. (2017). Exosomes: therapy delivery tools and biomarkers of diseases. *Pharmacol. Ther.* **174**, 63–78.
- Betts, M.R., Price, D.A., Brenchley, J.M., Lore, K., Guenaga, F.J., Smed-Sorensen, A., Ambrozak, D.R., Migueles, S.A., Connors, M., Roederer, M., et al. (2004). The functional profile of primary human antiviral CD8+ T cell effector activity is dictated by cognate peptide concentration. *J. Immunol.* **172**, 6407–6417.
- Boelen, L., Debebe, B., Silveira, M., Salam, A., Makinde, J., Roberts, C.H., Wang, E.C.Y., Frater, J., Gilmour, J., Twigger, K., et al. (2018). Inhibitory killer cell immunoglobulin-like receptors strengthen CD8(+) T cell-mediated control of HIV-1, HCV, and HTLV-1. *Sci. Immunol.* **3**, eaao2892.
- Bordner, A.J. (2010). Towards universal structure-based prediction of class II MHC epitopes for diverse allotypes. *PLoS One* **5**, e14383.
- Boudreau, J.E., Mulrooney, T.J., Le Ludec, J.B., Barker, E., and Hsu, K.C. (2016). KIR3DL1 and HLA-B density and binding calibrate NK education and response to HIV. *J. Immunol.* **196**, 3398–3410.
- Brackenridge, S., Evans, E.J., Toebes, M., Goonetilleke, N., Liu, M.K., di Gleria, K., Schumacher, T.N., Davis, S.J., McMichael, A.J., and Gillespie, G.M. (2011). An early HIV mutation within an HLA-B*57-restricted T cell epitope abrogates binding to the killer inhibitory receptor 3DL1. *J. Virol.* **85**, 5415–5422.
- Brander, C., and Walker, B.D. (1996). The HLA-class I restricted CTL response in HIV-1 infection: systematic identification of optimal epitopes. In *HIV Molecular Immunology Database 1996*, B. Korber, C. Brander, B. Haynes, R. Koup, J.P. Moore, B.D. Walker, P.M. D'Sousa, and G. Myers, eds. (Theoretical Biology and Biophysics Group, Los Alamos National Laboratory), pp. 50–60.
- Bricogne, G.B.E., Brandl, M., Flensburg, C., Keller, P., Paciorek, W., Roversi, P.S.A., Smart, O.S., Vornrhein, C., and Womack, T.O. (2011). Buster 2.11.2 (Global Phasing Ltd.).
- Burgess, R.R. (2009). Refolding solubilized inclusion body proteins. *Methods Enzymol.* **463**, 259–282.
- Carrington, M., and Alter, G. (2012). Innate immune control of HIV. *Cold Spring Harb Perspect. Med.* **2**, a007070.
- Chang, C.H., Kist, N.C., Chester, T.L., Sreenu, V.B., Herman, M., Luo, M., Lunn, D., Bell, J., Plummer, F.A., Ball, T.B., et al. (2015). HIV-infected sex workers with beneficial HLA-variants are potential hubs for selection of HIV-1 recombinants that may affect disease progression. *Sci. Rep.* **5**, 11253.
- Chang, S.C., Momburg, F., Bhutani, N., and Goldberg, A.L. (2005). The ER aminopeptidase, ERAP1, trims precursors to lengths of MHC class I peptides by a "molecular ruler" mechanism. *Proc. Natl. Acad. Sci. U S A* **102**, 17107–17112.
- Chen, H., Ndhlovu, Z.M., Liu, D., Porter, L.C., Fang, J.W., Darko, S., Brockman, M.A., Miura, T., Brumme, Z.L., Schneidewind, A., et al. (2012). TCR clonotypes modulate the protective effect of HLA class I molecules in HIV-1 infection. *Nat. Immunol.* **13**, 691–700.
- Chen, V.B., Arendall, W.B., 3rd, Headd, J.J., Keedy, D.A., Immormino, R.M., Kapral, G.J., Murray, L.W., Richardson, J.S., and Richardson, D.C. (2010). MolProbity: all-atom structure validation for macromolecular crystallography. *Acta Crystallogr. Section D, Biol. Crystallogr.* **66**, 12–21.
- de Vries, S.J., van Dijk, A.D., Krzeminski, M., van Dijk, M., Thureau, A., Hsu, V., Wassenaar, T., and Bonvin, A.M. (2007). HADDOCK versus HADDOCK: new features and performance of HADDOCK2.0 on the CAPRI targets. *Proteins* **69**, 726–733.
- Dominguez, C., Boelens, R., and Bonvin, A.M. (2003). HADDOCK: a protein-protein docking approach based on biochemical or biophysical information. *J. Am. Chem. Soc.* **125**, 1731–1737.
- Emsley, P., Lohkamp, B., Scott, W.G., and Cowtan, K. (2010). Features and development of Coot. *Acta Crystallogr. Section D, Biol. Crystallogr.* **66**, 486–501.
- Feeney, M.E., Tang, Y., Roosevelt, K.A., Leslie, A.J., McIntosh, K., Karthas, N., Walker, B.D., and Goulder, P.J. (2004). Immune escape precedes

breakthrough human immunodeficiency virus type 1 viremia and broadening of the cytotoxic T-lymphocyte response in an HLA-B27-positive long-term-nonprogressing child. *J. Virol.* 78, 8927–8930.

Gao, X., Bashirova, A., Iversen, A.K., Phair, J., Goedert, J.J., Buchbinder, S., Hoots, K., Vlahov, D., Altfeld, M., O'Brien, S.J., et al. (2005). AIDS restriction HLA allotypes target distinct intervals of HIV-1 pathogenesis. *Nat. Med.* 11, 1290–1292.

Gnann, J.W., Jr., Nelson, J.A., and Oldstone, M.B. (1987). Fine mapping of an immunodominant domain in the transmembrane glycoprotein of human immunodeficiency virus. *J. Virol.* 61, 2639–2641.

Gonzalez-Galarza, F.F., Takeshita, L.Y., Santos, E.J., Kempson, F., Maia, M.H., da Silva, A.L., Teles e Silva, A.L., Ghattaoraya, G.S., Alfirevic, A., Jones, A.R., et al. (2015). Allele frequency net 2015 update: new features for HLA epitopes, KIR and disease and HLA adverse drug reaction associations. *Nucleic Acids Res.* 43, D784–D788.

Goulder, P.J., Brander, C., Tang, Y., Tremblay, C., Colbert, R.A., Addo, M.M., Rosenberg, E.S., Nguyen, T., Allen, R., Trocha, A., et al. (2001). Evolution and transmission of stable CTL escape mutations in HIV infection. *Nature* 412, 334–338.

Goulder, P.J., Phillips, R.E., Colbert, R.A., McAdam, S., Ogg, G., Nowak, M.A., Giangrande, P., Luzzi, G., Morgan, B., Edwards, A., et al. (1997). Late escape from an immunodominant cytotoxic T-lymphocyte response associated with progression to AIDS. *Nat. Med.* 3, 212–217.

Goulder, P.J., Tang, Y., Pelton, S.I., and Walker, B.D. (2000). HLA-B57-restricted cytotoxic T-lymphocyte activity in a single infected subject toward two optimal epitopes, one of which is entirely contained within the other. *J. Virol.* 74, 5291–5299.

Goulder, P.J., and Walker, B.D. (2012). HIV and HLA class I: an evolving relationship. *Immunity* 37, 426–440.

Goulder, P.J., and Watkins, D.I. (2008). Impact of MHC class I diversity on immune control of immunodeficiency virus replication. *Nat. Rev. Immunol.* 8, 619–630.

Gubler, B., Daniel, S., Armandola, E.A., Hammer, J., Caillat-Zucman, S., and van Endert, P.M. (1998). Substrate selection by transporters associated with antigen processing occurs during peptide binding to TAP. *Mol. Immunol.* 35, 427–433.

Hillig, R.C., Hulsmeier, M., Saenger, W., Welfle, K., Misselwitz, R., Welfle, H., Kozerski, C., Volz, A., Uchanska-Ziegler, B., and Ziegler, A. (2004). Thermodynamic and structural analysis of peptide- and allele-dependent properties of two HLA-B27 subtypes exhibiting differential disease association. *J. Biol. Chem.* 279, 652–663.

HIV database (2020). HIV Molecular immunology 2020. <http://www.hivlanlgov/content/immunology>.

Hulsmeier, M., Welfle, K., Pohlmann, T., Misselwitz, R., Alexiev, U., Welfle, H., Saenger, W., Uchanska-Ziegler, B., and Ziegler, A. (2005). Thermodynamic and structural equivalence of two HLA-B27 subtypes complexed with a self-peptide. *J. Mol. Biol.* 346, 1367–1379.

Iglesias, M.C., Almeida, J.R., Fastenackels, S., van Bockel, D.J., Hashimoto, M., Venturi, V., Gostick, E., Urrutia, A., Wooldridge, L., Clement, M., et al. (2011). Escape from highly effective public CD8+ T-cell clonotypes by HIV. *Blood* 118, 2138–2149.

Iversen, A.K., Stewart-Jones, G., Learn, G.H., Christie, N., Sylvester-Hvid, C., Armitage, A.E., Kaul, R., Beattie, T., Lee, J.K., Li, Y., et al. (2006). Conflicting selective forces affect T cell receptor contacts in an immunodominant human immunodeficiency virus epitope. *Nat. Immunol.* 7, 179–189.

Joglekar, A.V., Liu, Z., Weber, J.K., Ouyang, Y., Jeppson, J.D., Noh, W.J., Lamothé-Molina, P.A., Chen, H., Kang, S.G., Bethune, M.T., et al. (2018). T cell receptors for the HIV KK10 epitope from patients with differential immunologic control are functionally indistinguishable. *Proc. Natl. Acad. Sci. U S A* 115, 1877–1882.

Kessler, J.H., Khan, S., Seifert, U., Le Gall, S., Chow, K.M., Paschen, A., Bres-Vloemans, S.A., de Ru, A., van Montfort, N., Franken, K.L., et al. (2011). An-

tigen processing by nardilysin and thimet oligopeptidase generates cytotoxic T cell epitopes. *Nat. Immunol.* 12, 45–53.

Kabsch, W. (2010). Xds. *Acta Crystallogr. Section D, Biol. Crystallogr.* 66, 125–132.

Kiepiela, P., Ngumbela, K., Thobakgale, C., Ramduth, D., Honeyborne, I., Moodley, E., Reddy, S., de Pierres, C., Mncube, Z., Mkhwanazi, N., et al. (2007). CD8+ T-cell responses to different HIV proteins have discordant associations with viral load. *Nat. Med.* 13, 46–53.

Kist, N.C., Lambert, B., Campbell, S., Katzourakis, A., Lunn, D., Lemey, P., and Iversen, A.K.N. (2020). HIV-1 p24Gag adaptation to modern and archaic HLA-allele frequency differences in ethnic groups contributes to viral subtype diversification. *Virus Evol.* 6, veaa085.

Kloverpris, H.N., Stryhn, A., Harndahl, M., van der Stok, M., Payne, R.P., Matthews, P.C., Chen, F., Riddell, L., Walker, B.D., Ndung'u, T., et al. (2012). HLA-B*57 Micropolyorphism shapes HLA allele-specific epitope immunogenicity, selection pressure, and HIV immune control. *J. Virol.* 86, 919–929.

Kuipers, J.G., Raybourne, R., Williams, K.M., Zeidler, H., and Yu, D.T. (1996). Requirements for HLA-B*2705-binding peptides with special regard to the transporter associated with antigen processing (TAP). *Clin. Exp. Rheumatol.* 14, 523–529.

Ladell, K., Hashimoto, M., Iglesias, M.C., Wilmann, P.G., McLaren, J.E., Gras, S., Chikata, T., Kuse, N., Fastenackels, S., Gostick, E., et al. (2013). A molecular basis for the control of preimmune escape variants by HIV-specific CD8+ T cells. *Immunity* 38, 425–436.

Lauvau, G., Kakimi, K., Niedermann, G., Ostankovitch, M., Yotnda, P., Firat, H., Chisari, F.V., and van Endert, P.M. (1999). Human transporters associated with antigen processing (TAPs) select epitope precursor peptides for processing in the endoplasmic reticulum and presentation to T cells. *J. Exp. Med.* 190, 1227–1240.

Lichterfeld, M., Kavanagh, D.G., Williams, K.L., Moza, B., Mui, S.K., Miura, T., Sivamurthy, R., Allgaier, R., Pereyra, F., Trocha, A., et al. (2007). A viral CTL escape mutation leading to immunoglobulin-like transcript 4-mediated functional inhibition of myelomonocytic cells. *J. Exp. Med.* 204, 2813–2824.

Liebschner, D., Afonine, P.V., Baker, M.L., Bunkoczi, G., Chen, V.B., Croll, T.I., Hintze, B., Hung, L.W., Jain, S., McCoy, A.J., et al. (2019). Macromolecular structure determination using X-rays, neutrons and electrons: recent developments in Phenix. *Acta Crystallogr. D Struct. Biol.* 75, 861–877.

Lock, C., Smilek, D., Gautam, A., Vaysburd, M., Dwivedy, S., and McDevitt, H. (1991). Competitive inhibition of antigen presentation in animal models of autoimmune disease. *Semin. Immunol.* 3, 247–255.

Martin, M.P., and Carrington, M. (2013). Immunogenetics of HIV disease. *Immunological Rev.* 254, 245–264.

Martin, M.P., Qi, Y., Gao, X., Yamada, E., Martin, J.N., Pereyra, F., Colombo, S., Brown, E.E., Shupert, W.L., Phair, J., et al. (2007). Innate partnership of HLA-B and KIR3DL1 subtypes against HIV-1. *Nat. Genet.* 39, 733–740.

Matthews, P.C., Koyanagi, M., Kloverpris, H.N., Harndahl, M., Stryhn, A., Akahoshi, T., Gatanaga, H., Oka, S., Juarez Molina, C., Valenzuela Ponce, H., et al. (2012). Differential clade-specific HLA-B*3501 association with HIV-1 disease outcome is linked to immunogenicity of a single Gag epitope. *J. Virol.* 86, 12643–12654.

Migueles, S.A., and Connors, M. (2015). Success and failure of the cellular immune response against HIV-1. *Nat. Immunol.* 16, 563–570.

Momburg, F., Roelse, J., Hammerling, G.J., and Neefjes, J.J. (1994a). Peptide size selection by the major histocompatibility complex-encoded peptide transporter. *J. Exp. Med.* 179, 1613–1623.

Momburg, F., Roelse, J., Howard, J.C., Butcher, G.W., Hammerling, G.J., and Neefjes, J.J. (1994b). Selectivity of MHC-encoded peptide transporters from human, mouse and rat. *Nature* 367, 648–651.

Nixon, D.F., Townsend, A.R., Elvin, J.G., Rizza, C.R., Gallwey, J., and McMichael, A.J. (1988). HIV-1 gag-specific cytotoxic T lymphocytes defined with recombinant vaccinia virus and synthetic peptides. *Nature* 336, 484–487.

- O'Connor, G.M., Vivian, J.P., Gostick, E., Pymm, P., Lafont, B.A., Price, D.A., Rossjohn, J., Brooks, A.G., and McVicar, D.W. (2015). Peptide-dependent recognition of HLA-B*57:01 by KIR3DS1. *J. Virol.* 89, 5213–5221.
- Paul, S., Weiskopf, D., Angelo, M.A., Sidney, J., Peters, B., and Sette, A. (2013). HLA class I alleles are associated with peptide-binding repertoires of different size, affinity, and immunogenicity. *J. Immunol.* 191, 5831–5839.
- Pereyra, F., Heckerman, D., Carlson, J.M., Kadie, C., Soghoian, D.Z., Karel, D., Goldenthal, A., Davis, O.B., DeZiel, C.E., Lin, T., et al. (2014). HIV control is mediated in part by CD8⁺ T-cell targeting of specific epitopes. *J. Virol.* 88, 12937–12948.
- Peruzzi, M., Parker, K.C., Long, E.O., and Malnati, M.S. (1996). Peptide sequence requirements for the recognition of HLA-B*2705 by specific natural killer cells. *J. Immunol.* 157, 3350–3356.
- Pettersen, E.F., Goddard, T.D., Huang, C.C., Couch, G.S., Greenblatt, D.M., Meng, E.C., and Ferrin, T.E. (2004). UCSF Chimera—a visualization system for exploratory research and analysis. *J. Comput. Chem.* 25, 1605–1612.
- Pettersen, E.F., Goddard, T.D., Huang, C.C., Meng, E.C., Couch, G.S., Croll, T.I., Morris, J.H., and Ferrin, T.E. (2021). UCSF ChimeraX: structure visualization for researchers, educators, and developers. *Protein Sci.* 30, 70–82.
- Phillips, R.E., Rowland-Jones, S., Nixon, D.F., Gotch, F.M., Edwards, J.P., Ogunlesi, A.O., Elvin, J.G., Rothbard, J.A., Bangham, C.R., Rizza, C.R., et al. (1991). Human immunodeficiency virus genetic variation that can escape cytotoxic T cell recognition. *Nature* 354, 453–459.
- Probst-Keppler, M., Hecht, H.J., Herrmann, H., Janke, V., Ocklenburg, F., Klempnauer, J., van den Eynde, B.J., and Weiss, S. (2004). Conformational restraints and flexibility of 14-mer peptides in complex with HLA-B*3501. *J. Immunol.* 173, 5610–5616.
- Purbhoo, M.A., Irvine, D.J., Huppa, J.B., and Davis, M.M. (2004). T cell killing does not require the formation of a stable mature immunological synapse. *Nat. Immunol.* 5, 524–530.
- Saric, T., Chang, S.C., Hattori, A., York, I.A., Markant, S., Rock, K.L., Tsujimoto, M., and Goldberg, A.L. (2002). An IFN- γ -induced aminopeptidase in the ER, ERAP1, trims precursors to MHC class I-presented peptides. *Nat. Immunol.* 3, 1169–1176.
- Saunders, P.M., Pymm, P., Pietra, G., Hughes, V.A., Hitchen, C., O'Connor, G.M., Loiacono, F., Widjaja, J., Price, D.A., Falco, M., et al. (2016). Killer cell immunoglobulin-like receptor 3DL1 polymorphism defines distinct hierarchies of HLA class I recognition. *J. Exp. Med.* 213, 791–807.
- Schmidt, J., Iversen, A.K., Tenzer, S., Gostick, E., Price, D.A., Lohmann, V., Distler, U., Bowness, P., Schild, H., Blum, H.E., et al. (2012). Rapid antigen processing and presentation of a protective and immunodominant HLA-B*27-restricted hepatitis C virus-specific CD8⁺ T-cell epitope. *PLoS Pathog.* 8, e1003042.
- Schmitt, L., Boniface, J.J., Davis, M.M., and McConnell, H.M. (1998). Kinetic isomers of a class II MHC-peptide complex. *Biochemistry* 37, 17371–17380.
- Schneidewind, A., Brockman, M.A., Sidney, J., Wang, Y.E., Chen, H., Suscovich, T.J., Li, B., Adam, R.I., Allgaier, R.L., Mothe, B.R., et al. (2008). Structural and functional constraints limit options for cytotoxic T-lymphocyte escape in the immunodominant HLA-B27-restricted epitope in human immunodeficiency virus type 1 capsid. *J. Virol.* 82, 5594–5605.
- Schneidewind, A., Brockman, M.A., Yang, R., Adam, R.I., Li, B., Le Gall, S., Rinaldo, C.R., Craggs, S.L., Allgaier, R.L., Power, K.A., et al. (2007). Escape from the dominant HLA-B27-restricted cytotoxic T-lymphocyte response in Gag is associated with a dramatic reduction in human immunodeficiency virus type 1 replication. *J. Virol.* 81, 12382–12393.
- Schneidewind, A., Brumme, Z.L., Brumme, C.J., Power, K.A., Rey, L.L., O'Sullivan, K., Gladden, A., Hempel, U., Kuntzen, T., Wang, Y.E., et al. (2009). Transmission and long-term stability of compensated CD8 escape mutations. *J. Virol.* 83, 3993–3997.
- Song, R., Lisovsky, I., Lebouche, B., Routy, J.P., Bruneau, J., and Bernard, N.F. (2014). HIV protective KIR3DL1/S1-HLA-B genotypes influence NK cell-mediated inhibition of HIV replication in autologous CD4 targets. *PLoS Pathog.* 10, e1003867.
- Steers, N.J., Currier, J.R., Kijak, G.H., di Targiani, R.C., Saxena, A., Marovich, M.A., Kim, J.H., Michael, N.L., Alving, C.R., and Rao, M. (2011). Cell type-specific proteasomal processing of HIV-1 Gag-p24 results in an altered epitope repertoire. *J. Virol.* 85, 1541–1553.
- Stewart-Jones, G.B., di Gleria, K., Kollnberger, S., McMichael, A.J., Jones, E.Y., and Bowness, P. (2005a). Crystal structures and KIR3DL1 recognition of three immunodominant viral peptides complexed to HLA-B*2705. *Eur. J. Immunol.* 35, 341–351.
- Stewart-Jones, G.B., Gillespie, G., Overton, I.M., Kaul, R., Roche, P., McMichael, A.J., Rowland-Jones, S., and Jones, E.Y. (2005b). Structures of three HIV-1 HLA-B*5703-peptide complexes and identification of related HLAs potentially associated with long-term nonprogression. *J. Immunol.* 175, 2459–2468.
- Tenzer, S., Crawford, H., Pymm, P., Gifford, R., Sreenu, V.B., Weimershaus, M., de Oliveira, T., Burgevin, A., Gerstoft, J., Akkad, N., et al. (2014). HIV-1 adaptation to antigen processing results in population-level immune evasion and affects subtype diversification. *Cell Rep.* 7, 448–463.
- Tenzer, S., Stoltze, L., Schonfisch, B., Dengjel, J., Muller, M., Stevanovic, S., Rammensee, H.G., and Schild, H. (2004). Quantitative analysis of prion-protein degradation by constitutive and immuno-20S proteasomes indicates differences correlated with disease susceptibility. *J. Immunol.* 172, 1083–1091.
- Tenzer, S., Wee, E., Burgevin, A., Stewart-Jones, G., Friis, L., Lamberth, K., Chang, C.H., Harndahl, M., Weimershaus, M., Gerstoft, J., et al. (2009). Antigen processing influences HIV-specific cytotoxic T lymphocyte immunodominance. *Nat. Immunol.* 10, 636–646.
- Tsumoto, K., Umetsu, M., Kumagai, I., Ejima, D., and Arakawa, T. (2003). Solubilization of active green fluorescent protein from insoluble particles by guanidine and arginine. *Biochem. biophysical Res. Commun.* 312, 1383–1386.
- Tynan, F.E., Borg, N.A., Miles, J.J., Beddoe, T., El-Hassen, D., Silins, S.L., van Zuylen, W.J., Purcell, A.W., Kjer-Nielsen, L., McCluskey, J., et al. (2005). High resolution structures of highly bulged viral epitopes bound to major histocompatibility complex class I. Implications for T-cell receptor engagement and T-cell immunodominance. *J. Biol. Chem.* 280, 23900–23909.
- van Endert, P. (2011). Post-proteasomal and proteasome-independent generation of MHC class I ligands. *Cell Mol. Life Sci. CMLS* 68, 1553–1567.
- van Endert, P.M., Riganelli, D., Greco, G., Fleischhauer, K., Sidney, J., Sette, A., and Bach, J.F. (1995). The peptide-binding motif for the human transporter associated with antigen processing. *J. Exp. Med.* 182, 1883–1895.
- Vivian, J.P., Duncan, R.C., Berry, R., O'Connor, G.M., Reid, H.H., Beddoe, T., Gras, S., Saunders, P.M., Olshina, M.A., Widjaja, J.M., et al. (2011). Killer cell immunoglobulin-like receptor 3DL1-mediated recognition of human leukocyte antigen B. *Nature* 479, 401–405.
- Wilson, J.D., Ogg, G.S., Allen, R.L., Goulder, P.J., Kelleher, A., Sewell, A.K., O'Callaghan, C.A., Rowland-Jones, S.L., Callan, M.F., and McMichael, A.J. (1998). Oligoclonal expansions of CD8⁺ T cells in chronic HIV infection are antigen specific. *J. Exp. Med.* 188, 785–790.
- Winn, M.D., Ballard, C.C., Cowtan, K.D., Dodson, E.J., Emsley, P., Evans, P.R., Keegan, R.M., Krissinel, E.B., Leslie, A.G., McCoy, A., et al. (2011). Overview of the CCP4 suite and current developments. *Acta Crystallogr. Section D, Biol. Crystallogr.* 67, 235–242.
- Xiao, Z., Ye, Z., Tadwal, V.S., Shen, M., and Ren, E.C. (2017). Dual non-contiguous peptide occupancy of HLA class I evoke antiviral human CD8 T cell response and form neo-epitopes with self-antigens. *Scientific Rep.* 7, 5072.
- York, I.A., Chang, S.C., Saric, T., Keys, J.A., Favreau, J.M., Goldberg, A.L., and Rock, K.L. (2002). The ER aminopeptidase ERAP1 enhances or limits antigen presentation by trimming epitopes to 8–9 residues. *Nat. Immunol.* 3, 1177–1184.

STAR★METHODS

KEY RESOURCES TABLE

REAGENT or RESOURCE	SOURCE	IDENTIFIER
Antibodies		
anti-human-CD4-APC-eFluor780	eBioscience	Cat#47-0049-42 RRID:AB_1272044
anti-human-CD8-PerCP	BD Biosciences	Cat#347314 RRID:AB_400280
anti-human-CD28	BioLegend	Cat# 302901 RRID:AB_314303
anti-human-CD49d	BioLegend	Cat# 304301 RRID:AB_314427
anti-human-CD107a-FITC	BioLegend	Cat#328605 RRID:AB_1186058
anti-human-IFN- γ -PE-Cy7	BioLegend	Cat#502527 RRID:AB_1626154
anti-human-TNF- α -APC	BioLegend	Cat# 502913 RRID:AB_315265
Anti-human-IL-2-PE	BioLegend	Cat# 500306 RRID:AB_315093
anti-human CD3-ECD	Beckman Coulter	Cat# IM2705U RRID:AB_130860
Live Dead Violet Viability Dye	ThermoFisher	Cat#L34955
Bacterial and virus strains		
<i>E. coli</i> DH5a	ThermoFisher	Cat#18258012
One Shot™ BL21(DE3)pLysS <i>E. coli</i>	ThermoFisher	Cat#C606003
Biological samples		
HLA B*27+ patient samples	Department of Infectious Diseases, Rigshospitalet, Denmark	Patient 1 to 10
Chemicals and recombinant proteins		
Trypsin EDTA	SigmaAldrich	Cat#59428C
Recombinant HLA B*27:05	This paper	N/A
Human IL-2	SigmaAldrich	Cat# I17002
Human IL-15	SigmaAldrich	Cat# I8648
Brefeldin A	BioLegend	Cat#420601
Monensin	BioLegend	Cat#420701
Phorbol myristate acetate	SigmaAldrich	Cat#P8139
Ionomycin	SigmaAldrich	Cat#I9657
Mouse IL-3	BioLegend	Cat#575502
HLA-B*27*05-PE Dextramers	Immudex	Custom
HLA-B*27*05-APC Dextramers	Immudex	Custom
KRWI (KI4)	Schafer-N	Custom
KRWII (KI5)	Schafer-N	Custom
KRWIIL (KL6)	Schafer-N	Custom
KRWIILG (KG7)	Schafer-N	Custom
KRWIILGL (KL8)	Schafer-N	Custom
KRWIILGLNKI (KI11)	Schafer-N	Custom
KRWIILGLNKIVR (KR13)	Schafer-N	Custom
KRWIILGLNKIVRM (KM14)	Schafer-N	Custom
Deposited data		
Crystal Structure Of HLA-B*2705 Complexed With the self-Peptide TIS from EGF-response factor 1	Hulsmeyer et al., 2005	PDB ID: 1W0V
Crystal structures and KIR3DL1 recognition of three immunodominant viral peptides complexed to HLA-B2705.	Stewart-Jones et al., 2005a	PDB ID: 2BSS
KIR3DL1 in complex with HLA-B*5701	Vivian et al., 2011	PDB ID: 3VH8

(Continued on next page)

Continued

REAGENT or RESOURCE	SOURCE	IDENTIFIER
HLA-B*27:05 presenting an HIV-1 6mer peptide	This Paper	PDB ID: 6VQZ
HLA-B*27:05 presenting an HIV-1 7mer peptide	This Paper	PDB ID: 6VQY
HLA-B*27:05 presenting an HIV-1 8mer peptide	This Paper	PDB ID: 6VQD
HLA-B*27:05 presenting an HIV-1 11mer peptide	This Paper	PDB ID: 6VPZ
HLA-B*27:05 presenting an HIV-1 13mer peptide	This Paper	PDB ID: 6VQE
HLA-B*27:05 presenting an HIV-1 14mer peptide	This Paper	PDB ID: 6VQ2

Experimental models: Cell lines

T2	ATCC	Cat#CRL-1992
Ba/F3	DSMZ	Cat# ACC 300

Oligonucleotides

GAG1 (round 1 (R1)) 728–751 (HIV numbering)	Chang et al., Sci. Rep, https://doi.org/10.1038/srep11253	Custom Synthesis
GAG3 (R1) 1941–1916 (HIV _{HXB2} numbering)	Chang et al., Sci. Rep, https://doi.org/10.1038/srep11253	Custom Synthesis
GAG2 (R2) 763–788 (HIV _{HXB2} numbering)	Chang et al., Sci. Rep, https://doi.org/10.1038/srep11253	Custom Synthesis
GAG4 (R2) 1911–1884 (HIV _{HXB2} numbering)	Chang et al., Sci. Rep, https://doi.org/10.1038/srep11253	Custom Synthesis

Recombinant DNA

HLA-B25:05-pGMT7 plasmid	Simon Kollnberger (co-author), https://doi.org/10.1002/eji.200425724 2005	Custom Synthesis
--------------------------	---	------------------

Software and algorithms

ChimeraX	Pettersen et al., 2021	https://www.cgl.ucsf.edu/chimerax/
Chimera v1.1.3	Pettersen et al., 2004	https://www.cgl.ucsf.edu/chimera/
Phenix v1.16	Liebschner et al., 2019	www.phenix-online.org
Coot v0.9.5	Emsley et al., 2010	https://www2.mrc-lmb.cam.ac.uk/personal/pemsley/coot/
PyMOL v2.3	The PyMOL Molecular Graphics System, Version 2.3 Schrödinger, LLC	https://pymol.org/2/
PISA	European Bioinformatics Institute	https://www.ebi.ac.uk/pdbe/prot_int/pistart.html
CCP4 v7.1	Winn et al., 2011	https://www.ccp4.ac.uk
XDS	Kabsch, 2010	https://xds.mr.mpg.de
HADDOCK v2.4	de Vries et al., 2007; Dominguez et al., 2003	https://wenmr.science.uu.nl/haddock2.4/
Summit v4.3	Beckman Coulter (Dako Cytomation)	https://www.beckman.com
Prism v9.0	Graphpad	https://www.graphpad.com/scientific-software/prism/
R v4.0.5	R Core Team., 2020	https://www.r-project.org
Stat Trek		https://stattrek.com

RESOURCE AVAILABILITY

Lead contact

Further information and requests for resources and reagents should be directed to and fulfilled by the lead contact, Astrid K.N. Iversen (astrid.iversen@ndcn.ox.ac.uk).

Materials availability

This study did not generate new unique reagents. The structures were deposited in the Protein Data Bank (PDB: 6VQZ for HLA-B*27:05-KL6; PDB: 6VQY for HLA-B*27:05-KG7; PDB: 6VQD for HLA-B*27:05-KL8; PDB: 6VPZ for HLA-B*27:05-KI11; PDB: 6VQE for HLA-B*27:05-KR13; and PDB: 6VQ2 for HLA-B*27:05-KM14).

Data and code availability

All data reported in this paper will be shared by the lead contact upon request. This paper does not report original code. Any additional information required to reanalyse the data reported in this paper is available from the lead contact upon request.

EXPERIMENTAL MODELS AND SUBJECT DETAILS

Patients and HLA genotyping

Patients with chronic HIV-1 infection were recruited from the Department of Infectious Diseases, Rigshospitalet, Denmark. All patients were female and were between 24 and 43 years of age. All patients gave written informed consent and were studied according to the regulations of the Danish Board of Medical Ethics. HLA genotyping was performed using a multiplex PCR (Dynal Biotech). Ten patients were found to carry the HLA-B*27:05 allele (Table S3).

METHOD DETAILS

Peptide synthesis and purification

Peptides were synthesized using an MK-IV peptide synthesizer (Schafer-N) and separated at > 98% purity using a JupiterProteo C12 column (Phenomenex)(Tenzer et al., 2009).

Proteasome purification and *in vitro* digestions

Constitutive proteasomes and immunoproteasomes (20S) were purified from LCL721.174 and LCL721 EBV-transformed human B cell lines, respectively (Tenzer et al., 2004). *In vitro* digestions with purified constitutive proteasomes and immunoproteasomes were performed at a substrate:enzyme ratio of 1,000:1 for 1, 2, 4, or 6 h. All peptide digestions in one experimental set were performed on the same day. Data were reported after 4 h, at which time < 40% of the initial substrate was degraded in all experiments, allowing the detection of all cleavage products while minimizing the effects of repeated proteasomal digestions.

Analysis of peptide digests by mass spectrometry

Peptide digests were analyzed via capillary liquid chromatography (LC) using a Waters NanoAcquity UPLC System (Waters) and via mass spectrometry (MS) using a Q-ToF Premier Mass Spectrometer (Waters) (Tenzer et al., 2009). Each sample was analyzed in triplicate. LC-MS^E data were processed using the ProteinLynx Global Server (Waters). The mass error tolerance values were typically < 5 ppm. Mass spectrometric fragment intensity was used as a surrogate marker for quantity(Tenzer et al., 2009).

TAP-peptide binding assays and ERAP1/2 digestions

TAP-peptide competitive binding assays and normalization of results, and ERAP1/2 digestions were performed as described previously (Tenzer et al., 2009).

Expression, purification, and crystallization of HLA-B*27:05-peptide complexes

HLA-B*27:05 heavy chain and β 2M proteins were expressed and purified as described previously (Burgess, 2009; Tenzer et al., 2009) and refolded with peptide using a rapid dilution method (Tsumoto et al., 2003). Heterotrimeric complexes were purified via size exclusion using a HiLoad 26/600 Superdex 75 pg column fitted to an AKTA Purifier FPLC System (GE Healthcare). Eluent fractions corresponding to absorbance peaks were examined via SDS-PAGE. Heterotrimeric complexes were then purified again via size exclusion using a Superdex 75 10/300 GL column fitted to an AKTA Purifier FPLC System (GE Healthcare). Correctly refolded heterotrimers were concentrated to > 10 mg/mL for crystallization trials using Amicon Ultra-0.5 Centrifugal Filter Units with Ultracel-10 Membranes (Merck Millipore). Optimal protein concentrations were determined for each complex using a PCT Pre-Crystallization Test (Hampton Research). Correctly refolded heterotrimers that did not crystallize were examined using mass spectrometry. Crystallization was carried out using the sitting-drop vapor-diffusion method. Briefly, crystallization screen reagents (Hampton Research) were dispensed into a CrystalQuick 96 Well Sitting Drop Plate (Greiner) using a Hydra eDrop II (Thermo Fisher Scientific), and 10 nL of protein was dispensed as a sitting drop in each well after mixing with 10 nL of the corresponding well buffer using a Microsys Liquid Handler (Cartesian Technologies). Crystal screens were stored at 4°C using a Protein Crystallization Imager (Formulatrix). Crystals obtained from the screens were immersed in reservoir buffer containing 20% glycerol as a cryoprotectant and vitrified at 100 K in liquid nitrogen. X-ray diffraction was carried out on beamlines at the European Synchrotron Radiation Facility, Grenoble, France (www.esrf.eu) or at the Diamond Light Source, Didcot, UK (www.diamond.ac.uk).

Modeling of HLA-B*27:05-peptide complexes and the interaction between HLA-B*27:05 and KIR3DL1*001

HLA-B*27:05-peptide models were constructed using molecular replacement using PDB ID: 1W0V with the original peptide was omitted (Hulsmeyer et al., 2005). Manual building and refinement were carried out using Coot (Emsley et al., 2010), Buster (Bricogne et al., 2011), and Phenix (Adams et al., 2010). Simulated annealing was performed during the initial refinement process to avoid bias from the reference model. Non-crystallographic symmetry restraints were used for the KL6 and KG7 structures, in which the asymmetric unit comprised two HLA-B*27:05-peptide complexes, and these restraints were removed for the final round of refinement (Pettersen et al., 2004) (Kabsch, 2010) (Winn et al., 2011) (Pettersen et al., 2021). Model validation was carried out using MolProbity (Chen et al., 2010). Figures were prepared using the PyMol Molecular Graphics System (Schrödinger Inc.). The Adaptive Poisson-Boltzmann Solver (APBS) plugin was used to calculate electrostatic potentials for the models shown by solving the Poisson-Boltzmann equation (Baker et al., 2001). B-factors (average mean atomic displacement from the position in the refined structure) were normalized using the HLA heavy-chain data across all models to standardize the average B-factor of the HLA among the six structures, and peptide B-factors were compared to give a measure of relative local disorder.

The HLA-B*27:05 interaction with KIR3DL1*001 for the KK10 and KI11 epitopes was modeled using PDB entries 2BSS and 3VH8 for HLA-B*27:05-KK10 and KIR3DL1*001, respectively, along with our structure for HLA-B*27:05-KI11 (PDB ID: 6VPZ). Docking was modeled using HADDOCK (de Vries et al., 2007; Dominguez et al., 2003). Restraints included all contacts at the KIR3DL1*001-HLA-B*57:01 interface, excluding the peptide contact at position 8 listed previously (Vivian et al., 2011) (Liebschner et al., 2019). Passive residues were defined automatically. Manual error checking was undertaken using Coot (Emsley et al., 2010), guided by the electron density submitted for the KIR3DL1*001-HLA-B*57:01 complex (PDB ID: 3VH8).

Ex vivo staining of PBMCs with HLA-B*27:05-peptide dextramers

PBMCs were stained with LIVE/DEAD Fixable Violet (Thermo Fisher Scientific). Cells were then washed twice and incubated with HLA-B*27:05-peptide dextramers as per the manufacturer's protocol (Immudex). Surface markers were identified using anti-CD3-ECD (Beckman Coulter), anti-CD4-APC-eFluor780 (eBioscience), and anti-CD8-PerCP (BD Biosciences). Cells were then washed again and fixed with 1% formaldehyde for a minimum of 1 h. Non-identical HLA-A*2:01-peptide dextramers containing an irrelevant epitope were used as gating controls. Unstained and single-stained cells were used to determine compensation values. Samples were acquired using a CyAn ADP Analyzer (Beckman Dako Cytomation), and data were analyzed using FlowJo software (Tree Star).

Amplification and sequencing of HIV-1 p24 Gag

DNA was extracted from approximately 10^5 PBMCs using a Gentra Puregene Blood Core Kit A (Qiagen). PCR amplification of ~1,200 bases spanning the HIV-1 p17-p24 region was performed as described previously (Chang et al., 2015). Amplicons were cloned using a TOPO TA Cloning Kit (Thermo Fisher Scientific) and sequenced using a 3730 DNA Analyzer (Applied Biosystems). Ten clones were analyzed per sample. Forward and reverse sequence reads were assembled and proofread using Sequencher (Gene Codes Corporation) and aligned and manually edited using MacClade (Sinauer Associates).

Standard and competition IFN- γ ELISpot assays

G12C cells were expanded as described previously (Iversen et al., 2006) and rested for 2 days in fresh medium supplemented with IL-2 (20 IU/mL) and IL-15 (25 ng/mL) before testing in IFN- γ ELISpot assays (Merck Millipore) (Tenzer et al., 2009, 2014). TAP-deficient T2 cells were transfected with HLA-B*27:05 to generate T2-HLA-B*27:05 cells (Kuipers et al., 1996). These cells were used in competition assays to minimize the potentially confounding effects of internally loaded peptides and other HLA class I and class II molecules. T2-HLA-B*27:05 cells were incubated for 30 min at 37°C with various concentrations of a given epitope-form peptide, corresponding to molar ratios of 1, 10, 50, 250, 400, and 800 relative to the KK10 peptide, which was then added at the EC50 concentration (Altfeld et al., 2000). The EC50 concentration was determined in preliminary ELISpot assays as the concentration required to elicit half-maximal IFN- γ production (Tenzer et al., 2009, 2014). Samples were tested in triplicate or quadruplicate. G12C responses were expressed as spot-forming units per 10^6 cells. Standard ex vivo IFN- γ ELISpot assays were performed as described previously (Tenzer et al., 2009, 2014).

Standard and competition ICS assays

PBMCs were stimulated in a 96-well plate with various concentrations of peptide (KK10), anti-CD28 (1 μ g/mL), and anti-CD49d (1 μ g/mL) for 6 h in the presence of anti-CD107a-FITC (BioLegend). Cytokine secretion was blocked with brefeldin A (5 μ g/mL; BioLegend) and monensin (2 μ M; BioLegend). Negative control wells contained anti-CD28 (1 μ g/mL) and anti-CD49d (1 μ g/mL). Positive control wells contained anti-CD28 (1 μ g/mL), anti-CD49d (1 μ g/mL), phorbol myristate acetate (2.5 ng/mL), and ionomycin (25 ng/mL). Cells were then stained with LIVE/DEAD Fixable Violet (Thermo Fisher Scientific), fixed/permeabilized using a Cytofix/Cytoperm Kit (BD Biosciences), and stained with anti-CD3-ECD (Beckman Coulter), anti-CD8-PerCP (BD Biosciences), anti-IFN- γ -PE-Cy7 (BioLegend), anti-TNF- α -APC (BioLegend), and anti-IL-2-PE (BioLegend). Unstained and single-stained cells were used to determine compensation values. Samples were acquired using a Cyan ADP Analyzer (Beckman Dako Cytomation), and data were analyzed using Summit software (Beckman Dako Cytomation). Competition assays were performed similarly using the truncated epitope-form peptides at molar ratios of 1, 10, 50, 250, 400, and 800 relative to the KK10 peptide, which was added at the calculated EC50 concentration after

30 min at 37°C. Control wells contained truncated epitope-form peptides alone or the KK10 peptide alone. Samples were tested in duplicate.

KIR3DL1*001 binding assay

Parental or KIR3DL1*001-transfected BA/F3 cells were expanded in the presence of mouse IL-3 (0.5 ng/mL) as described previously (Stewart-Jones et al., 2005a). Each line was stained with LIVE/DEAD Fixable Violet (Thermo Fisher Scientific). Cells were then washed twice and incubated with HLA-B*27:05-peptide dextramers as per the manufacturer's protocol (Immudex). The parental line was used as a control for each condition. Samples were tested in duplicate. Cells were then washed again and fixed with 1% formaldehyde for a minimum of 1 h. Samples were acquired using a Cyan ADP Analyzer (Beckman Dako Cytomation), and data were analyzed using FlowJo software (Tree Star).

QUANTIFICATION AND STATISTICAL ANALYSIS

Statistical analyses were performed using the indicated tests in Excel (Microsoft), Prism (GraphPad), R (<https://www.r-project.org>), or Stat Trek (<https://stattek.com>). Comparisons were considered significant at $P < 0.05$.

Supplemental information

Epitope length variants

balance protective immune responses

and viral escape in HIV-1 infection

Phillip Pymm, Stefan Tenzer, Edmund Wee, Mirjana Weimershaus, Anne Burgevin, Simon Kollnberger, Jan Gerstoft, Tracy M. Josephs, Kristin Ladell, James E. McLaren, Victor Appay, David A. Price, Lars Fugger, John I. Bell, Hansjörg Schild, Peter van Endert, Maria Harkiolaki, and Astrid K.N. Iversen

Figure S1

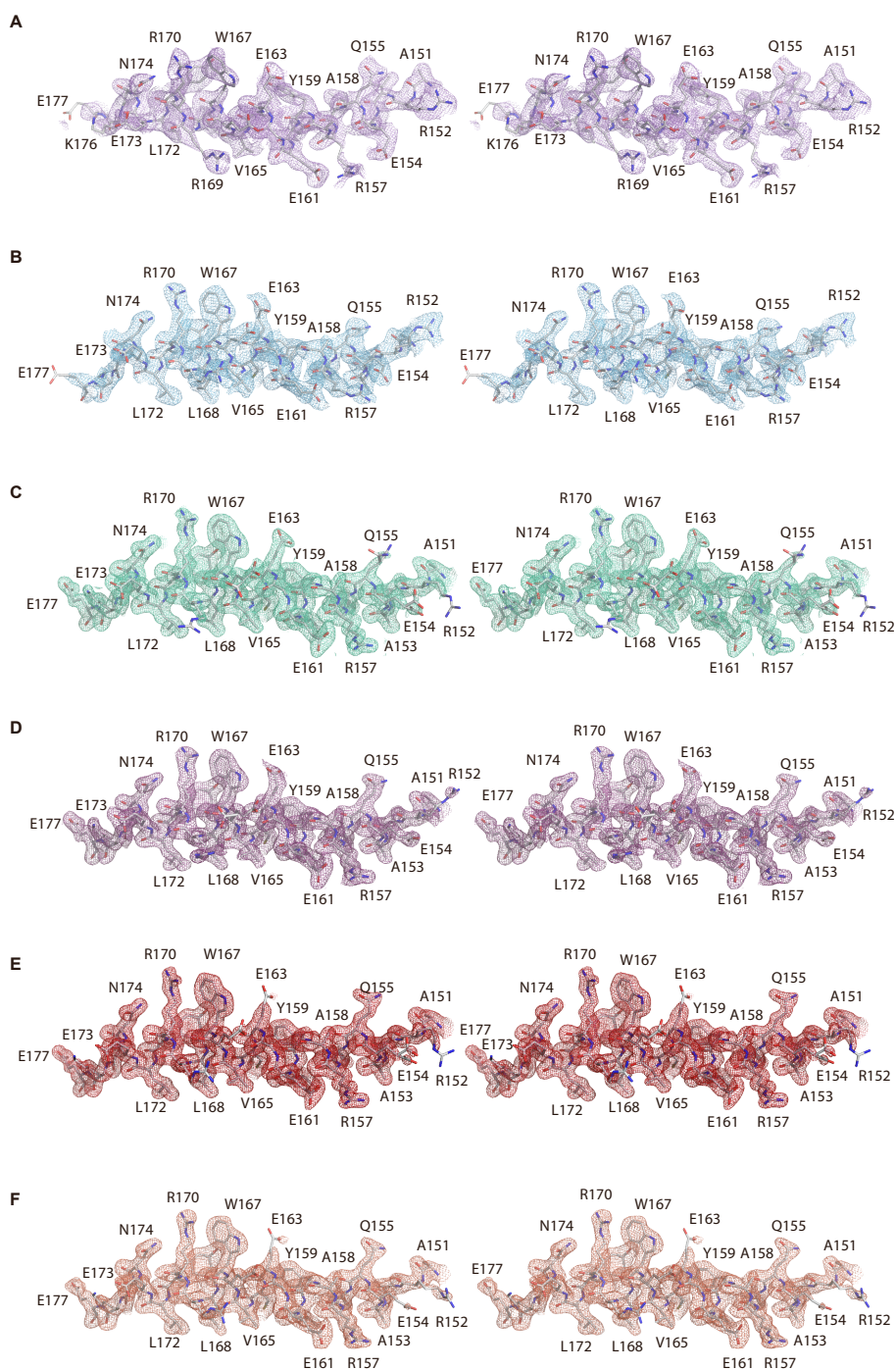


Figure S1. Stereo images of the electron density of residues 150 to 177 of the $\alpha 2$ helix of the HLA-B*27:05 heavy chain consisting of the following amino acid residue sequence in single-letter amino acid code: ARVAEQLRAYLEGECEVWLRR

YLENGKE, related to Figure 2. Density shown is taken from the refined 2mFo-DFc map within 1.6Å of atoms with a 1.2σ cutoff. Selected amino acid residues are labelled for HLA-B*27:05 KRWIIL (**A**), HLA-B*27:05 KRWILG (**B**), HLA-B*27:05 KRWIILGL (**C**), HLA-B*27:05 KRWIILGLNKI (**D**), HLA-B*27:05 KRWIILGLNKIVR (**E**), HLA-B*27:05 KRWIILGLNKIVRM (**F**).

Figure S2

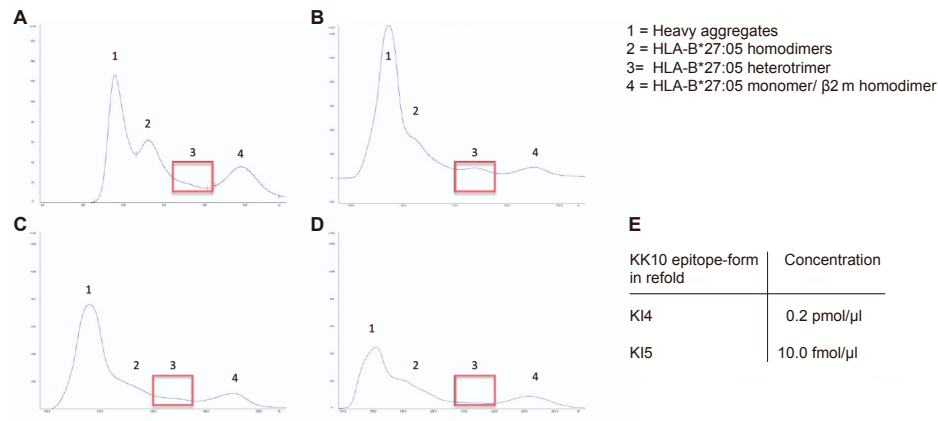


Figure S2. FPLC analyses of KI4, KI5, and WK8 refolds with HLA-B*27:05, related to Figures 2. (A–E) Fast protein liquid chromatography (FPLC) analyses of refolds containing the HLA-B*27:05 heavy chain and β 2m with no peptide (control) (A), KI4 (B), KI5 (C), or WK8 (D). (E) Peptide concentration in the KI4 and KI5 refolds. The refolds were diluted 1:100 in 1% formic acid to free the peptides before mass spectrometry. The red box indicates the HLA-B*27:05 heterotrimer (HLA-B27:05- β 2m-peptide).

Figure S3

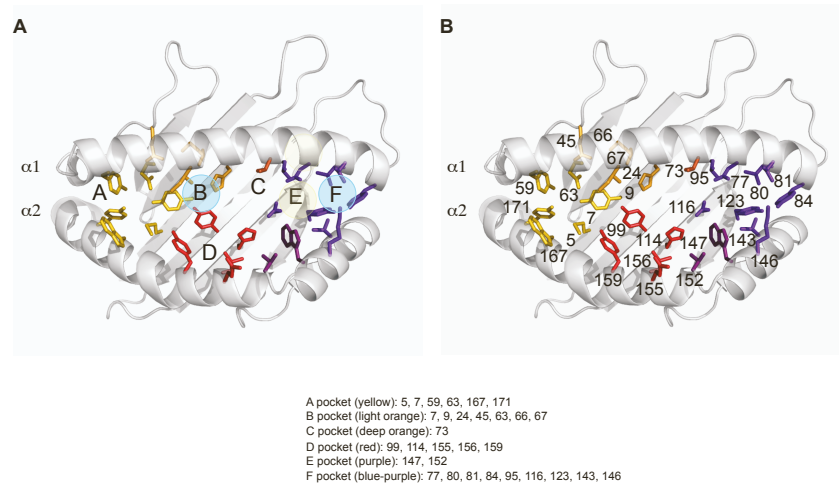


Figure S3. Overview of the HLA-B*27:05 binding groove, related to Figure 2. (A) Top-view of the peptide-binding groove of HLA-B*27:05 showing the A-, B-, C-, D-, E-, and F-pockets. The B- and F-pockets are indicated by light-blue disks, and the E-pocket is indicated by a light-yellow disk. **(B)** Top-view of the peptide-binding groove of HLA-B*27:05 showing the interacting amino acid residues for each pocket, colored and numbered as indicated in the key.

Figure S4

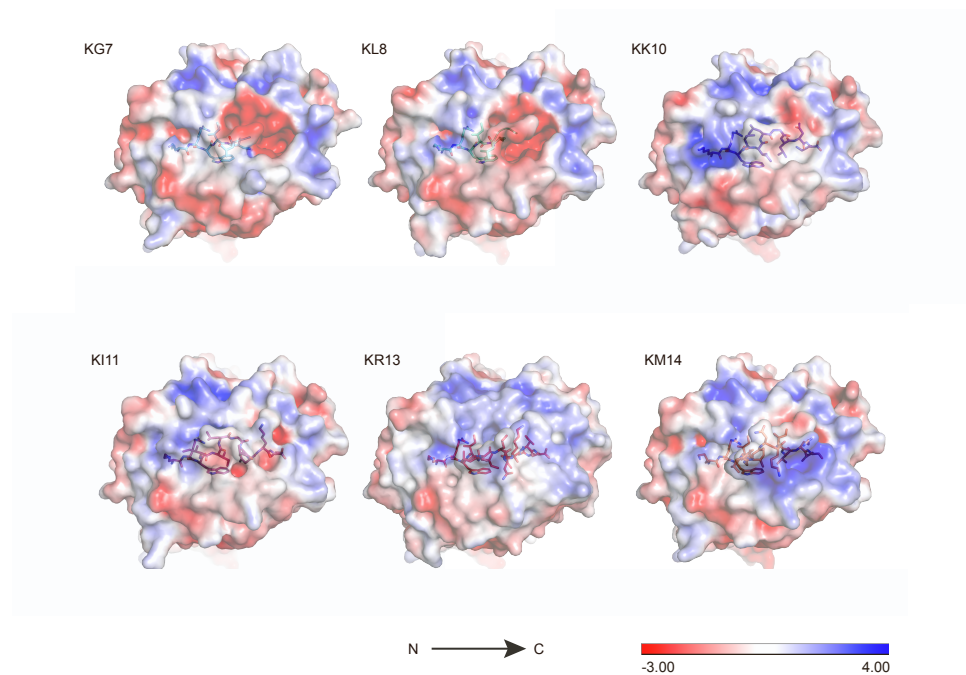


Figure S4. Electrostatic analyses of HLA-B*27:05-peptide complexes, related to Figure 3. Colours represent the electrostatic potential on the surface of each HLA-B*27:05-peptide complex as indicated in the key.

Figure S5

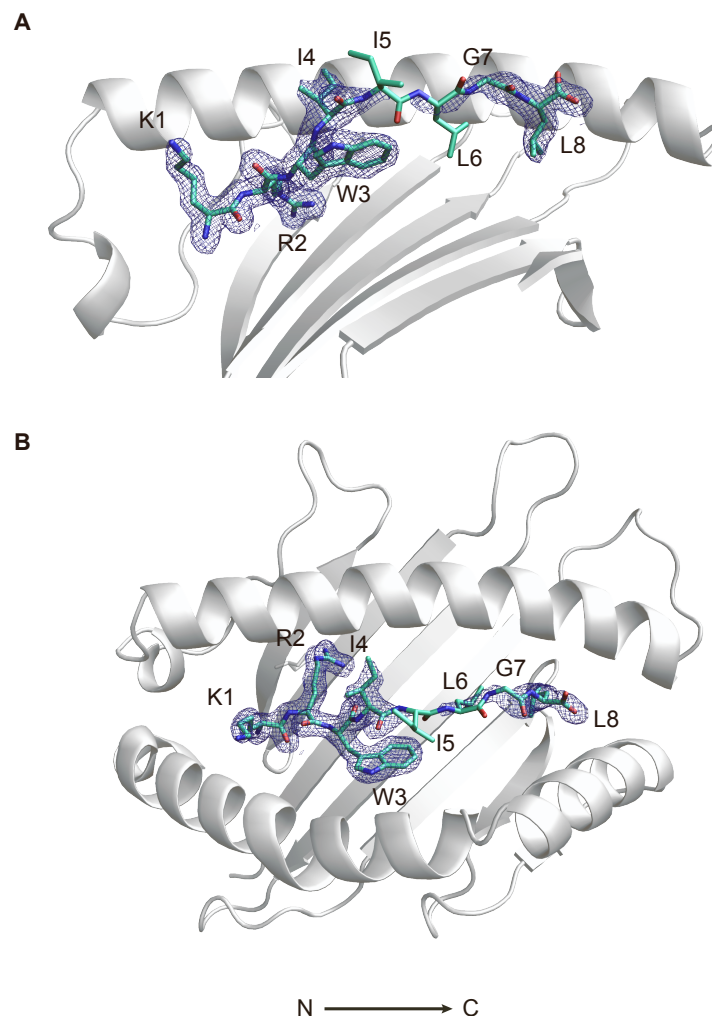
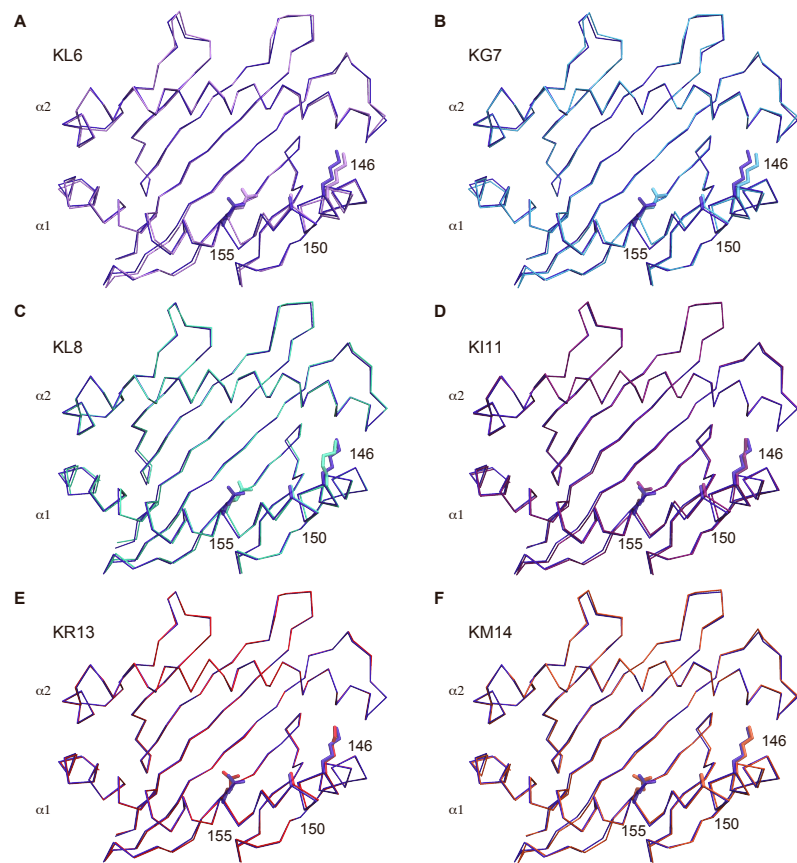


Figure S5. Images of the refined density of the KRWIILGL-SP (KL8-SP) structure, related to Figures 2 and 3. The scaled map was put through one round of refinement with the alternate model around the peptide at 1.0 sigma; (A) side-view and (B) top-view. The figures show occupancy at the C-terminus including Gly7 and a very small amount of density for positions 5 and 6. We estimate that there is ~10% occupancy for these

residues and that the better density at the C-terminus likely is explained by this position being filled with an arginine from the refolding buffer in the "normal" KL8 model.

Figure S6



Structure colour key: KK10 = purple, KL6 = mauve, KG7 = baby blue, KL8 = turquoise, KI1 = magenta, KR13 = red, KM14 = orange

Structure:	KL6	KG7	KL8	KI11	KR13	KM14
Residue						
146	0.8→	0.6→	0.5→	0.4↗	0.3↗	0.3↗
150	0.7→↓	0.5→↓	0.3→	0.4↗	0.4↗	0.2↗
155	1.2↗	1.2↗	0.6↗	0.5↗	0.4↗	0.4↗
←	Wider					
→	Narrower					
↑	Up from Platform					
↓	Towards Platform					
↖	N-Terminal					
↗	C-Terminal					

Figure S6. The positions of the HLA helices and key residues in all structures relative to the corresponding positions in the HLA-B*27:05-KK10 structure; (A), KL6 (B), KG7 (C), KL8, (D), KI11, (E), KR13, and, (F), KM14, related to Figures 2, 3 and 5. Each structure was overlaid on the α 1 helix of HLA-B*27:05-KK10 (purple). Changes in the positions of key residues (D146_{B27}, L150_{B27}, and S155_{B27}) are summarized in the bottom panel with distances measured in Å.

Figure S7

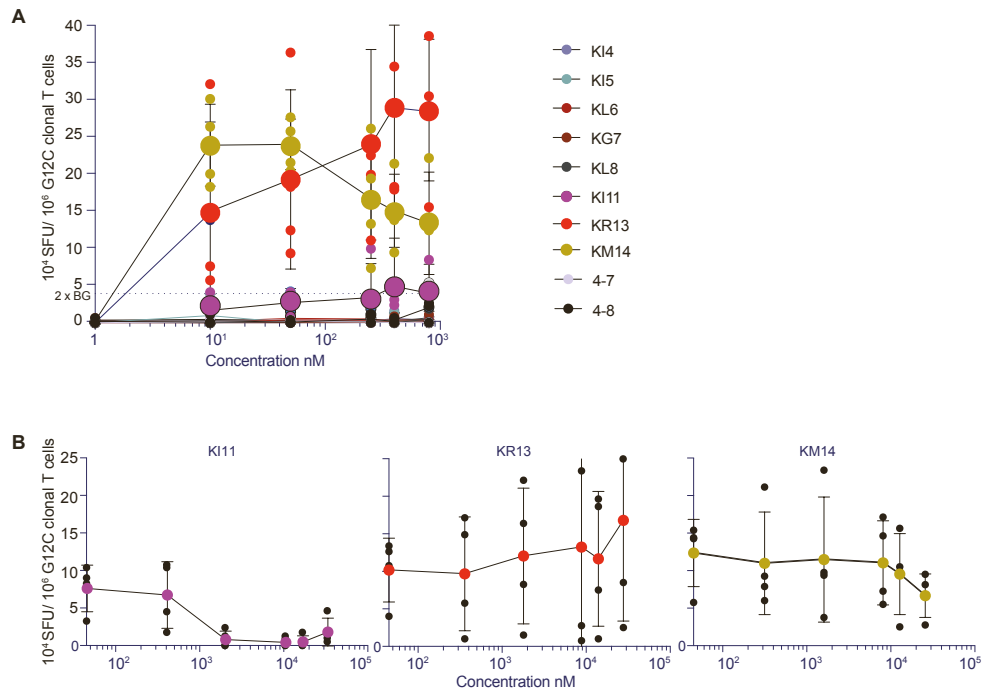


Figure S7. Analyses of G12C responses to extended KK10 epitope-form peptides.

(A) IFN- γ release by G12C in response to individual KK10-minitopes and two mixtures of KK10-minitopes at molar ratios of 1, 10, 50, 250, 400, and 800 relative to KK10, **related to Figure 6**. The KM14 response was likely affected at higher ratios by excess DMSO (final concentration > 1%). Small dots indicate experimental data. Large dots indicate mean values. The dotted line indicates twice the background response (BG). Error bars indicate SD. (B) IFN- γ release by G12C in response to KK10 at the EC50 concentration in the presence of KI11, KR13, or KM14 at molar ratios of 1, 10, 50, 250, 400, and 800 relative to KK10. The KM14 response was likely affected at higher ratios by excess DMSO (final concentration > 1%). Small dots indicate experimental data. Large dots indicate mean values. Twice the background response was subtracted per data

point. Error bars indicate SD. ELISpot data are shown as spot-forming units (SFU) per 10^6 cells (A, B).

Supplementary Tables 1 to 3

Table S1. Proteasomal production of KK10 epitope-forms

(related to Fig. 1)

WT, wildtype; K, R132K substitution; M, L136M substitution; KM, R132K and L136M substitutions; CP, constitutive proteasome (data shown as % of all fragments produced); IP, immunoproteasome (data shown as % of all fragments produced). Asterisks indicate trace amounts of a given epitope-form. Red indicates the presence of a CTL escape mutation in a given fragment.

KK10 epitope-form	p24 fragment VGEIYKRWIILGLNKIVRMYSPTSI Sequence	4h CP digest %	4h IP digest %
KM-14-WT	VGEIYKRWIILGLNKIVRM	3.6	0.2
KM-14-WT (GM18)	GEIYKRWIILGLNKIVRM	0.2	0
KR-13-WT	VGEIYKRWIILGLNKIVR	2	0
KR-13-WT (GR17)	GEIYKRWIILGLNKIVR	0.1	0
KI-11-WT	VGEIYKRWIILGLNKI	1	0
KI-11-WT (GI15)	GEIYKRWIILGLNKI	0.1	0
KK-10-WT (VK15)	VGEIYKRWIILGLNK	0.2	0.1
KL-8-WT	VGEIYKRWIILGL	4.6	7.7
KL-8-WT	GEIYKRWIILGL	1.9	2.7
KL-8-WT	EIYKRWIILGL	0.5	0.8
KL-8-WT	IYKRWIILGL	0.1	0.4
KL-8-WT	YKRWIILGL	0.1	0.1
KL-8-WT	KRWIILGL	0.7	5.2
KG-7-WT	VGEIYKRWIILG	1.8	0.5
KG-7-WT	GEIYKRWIILG	1.3	0.4
KG-7-WT	KRWIILG	0.6	0.1
KL-6-WT	VGEIYKRWIIL	10	8.8
KL-6-WT	GEIYKRWIIL	10.8	9
KL-6-WT	EIYKRWIIL	1.6	1.4
KL-6-WT	IYKRWIIL	0.4	0.3
KL-6-WT	KRWIIL	3.8	5.5
KI-5-WT	VGEIYKRWII	0.2	0.5
KI-5-WT	GEIYKRWII	0.2	0.9
KI-5-WT	IYKRWII	0.1	0.2
KI-5-WT	KRWII	0.1	0.1
KI-4-WT	VGEIYKRWI	0.2	0.1
KI-4-WT	GEIYKRWI	0.3	0.1

Total KK-10 epitope-form production	46.5	45.1
-------------------------------------	------	------

KK10 epitope form	p24 fragment VGEIYK K WII LGLNKIVRMYSPTSI Sequence	4h CP digest %	4h IP digest I %
KK-10-K	VGEIYK K WII LGLNK	0.5	0.0
KL-8-K	VGEIYK K WII LGL	7.3	0.1
KL-8-K	EIYK K WII LGL	0.1	0.0
KL-8-K	K WII LGL	0.0	0.003*
KL-6-K	VGEIYK K WII L	24.6	0.2
KL-6-K	GEIYK K WII L	1.4	0.006*
KL-6-K	K WII L	0.4	0.005*
KI-5-K	VGEIYK K WII	0.2	0.01*
KI-5-K	GEIYK K WII	0.0	0.002*
Total KK-10 epitope-form production		34.5	0.3

KK10 epitope form	p24 fragment VGEIYKRWII M GLNKIVRMYSPTSI Sequence	4h CP digest %	4h IP digest %
KL-8-M	VGEIYKRWII M GL	2.7	12.8
KL-8-M	KRWII M GL	0.2	3.4
KG-7-M	VGEIYKRWII M G	9.6	2
KG-7-M	EIYKRWII M G	0.0	0.04*
KG-7-M	KRWII M G	0.6	0.2
KM-6-M	VGEIYKRWII M	11.8	6.7
KM-6-M	GEIYKRWII M	0.4	0.3
KM-6-M	KRWII M	0.4	4.3
KI-5-M	VGEIYKRWII	0.5	5.6
KI-5-M	GEIYKRWII	0.0	0.6
Total KK-10 epitope-form production		26.2	35.94

KK10 epitope form	p24 fragment VGEIYK KWII MGLNKIVRMYSPTSI Sequence	4h CP digest %	4h IP digest %
KV-12-KM	GEIYK KWII MGLNKIV	0.2	0.1
KI-11-KM	VGEIYK KWII MGLNKI	0.2	0.1
KK-10-KM	KKWII MGLNK	0.2	0.2
KL-8-KM	VGEIYK KWII MGL	3.2	15.8
KL-8-KM	GEIYK KWII MGL	0.3	0.5
KL-8-KM	KKWII MGL	0.0	0.6
KM-6-KM	VGEIYK KWII M	16.5	13
KM-6-KM	GEIYK KWII M	0.7	0.5
KI-5-KM	VGEIYK KWII	1.1	8.1
KI-5-KM	GEIYK KWII	0.1	1.2
Total KK-10 epitope-form production		22.5	40.1

Table S2. Crystal data collection and refinement statistics (molecular replacement) (related to Fig. 2 and Fig. S1)

	HLA-B*27:05-KM14	HLA-B*27:05-KR13	HLA-B*27:05-KI11	HLA-B*27:05-KL8	HLA-B*27:05-KG7	HLA-B*27:05-KL6
Data collection						
Space group	P2 ₁ 2 ₁ 2 ₁	P2 ₁ 2 ₁ 2 ₁	P2 ₁ 2 ₁ 2 ₁	P2 ₁ 2 ₁ 2 ₁	P2 ₁	P2 ₁
Cell dimensions						
<i>a</i> , <i>b</i> , <i>c</i> (Å)	51.29, 82.81, 110.57	50.95, 82.65, 109.39	51.25, 83.07, 110.12	50.87, 82.71, 108.64	45.35, 129.86, 90.26	45.49, 130.52, 90.17
α , β , γ (°)	90, 90, 90	90, 90, 90	90, 90, 90	90, 90, 90	90, 104.38, 90	90, 104.41, 90
Resolution (Å)	66.28-2.25 (2.37-2.25)	46.18-1.77 (1.81-1.77)	66.32-2.10 (2.21-2.10)	54.32-1.88 (1.98-1.88)	87.44-2.57 (2.71-2.57)	87.33-2.25 (2.37-2.25)
<i>R</i> _{sym} or <i>R</i> _{merge}	0.44 (1.89)	0.07 (0.41)	0.21 (0.80)	0.12 (0.77)	0.23 (0.60)	0.09 (0.49)
<i>I</i> / σ <i>I</i>	7.8 (3.8)	13.7 (3.9)	8.4 (2.3)	15.6 (3.6)	5.6 (2.2)	6.7 (2.3)
Completeness (%)	100 (100)	99.8 (96.7)	100 (100)	100 (100)	100 (100)	98.1 (97.1)
Redundancy	12.4 (12.2)	6.1 (4.9)	7.1 (7.2)	14.2 (14.5)	5.2 (3.5)	2.5 (2.6)
Refinement						
No. reflections	23098 (3309)	45852 (2489)	28236 (4054)	38122 (5467)	32272 (4694)	47317 (6830)
<i>R</i> _{work} / <i>R</i> _{free}	17.5 / 23.0	16.1 / 18.6	19.0 / 23.5	17.2 / 20.6	21.1 / 23.9	20.0 / 24.3
No. atoms	3472	3639	3522	3731	6434	6521
Protein	3198	3245	3210	3211	6305	6406
Ligand/ion	12	12	6	18	12	0
Water	262	382	306	502	117	115
<i>B</i> -factors	28.65	26.37	20.64	27.60	28.39	39.81
Protein	28.22	25.03	20.21	26.31	28.46	39.94
Ligand/ion	39.20	42.43	26.09	35.24	33.23	N/A
Water	33.30	37.28	25.10	35.56	24.27	32.50
R.m.s. deviations						
Bond lengths (Å)	0.004	0.008	0.014	0.009	0.003	0.004
Bond angles (°)	0.69	0.97	1.22	0.92	0.61	0.79

Table S3. Patient details (related to Fig. 5)

Patient ID	KK10 response	Years infected	Viral load copies/ml	CD4 count cells/ μ l	Medication
1	yes	9 months	112,171	330	NA
2	yes	11 years, 5 months	91,258	630	NA
3	yes	16 years, 1 month	34,704	540	NA
4	yes	2 years, 4 months	16,625	760	NA
5	yes	1 year, 5 months	12,614	540	NA
6	yes	4 years, 2 months	39	419	Truvada, Efavirenz
7	no	19 years, 7 months	39	1,000	Viread, Kaletra
8	no	4 years	87,342	580	NA
9	no	6 years	190	470	Viramun, Kivexa
10	no	3 to 23 years*	1,843	190	NA

Information at the time of sampling. *The first positive test was 3 years before sampling, but patient 10 was likely infected 15–20 years earlier. NA, not applicable.